

Dark matter, fine-tuning and $(g - 2)_\mu$ in the pMSSM

M. van Beekveld^{1*}, W. Beenakker², M. Schutten^{2,4}, J. de Wit²

1 Rudolf Peierls Centre for Theoretical Physics, 20 Parks Road, Oxford OX1 3PU,
United Kingdom

2 THEP, Radboud University, Heyendaalseweg 135, 6525 AJ Nijmegen, the Netherlands

3 Institute of Physics, University of Amsterdam, Science Park 904, 1018 XE Amsterdam,
the Netherlands

4 Van Swinderen Institute for Particle Physics and Gravity, University of Groningen,
9747 AG Groningen, The Netherlands

* melissa.vanbeekveld@physics.ox.ac.uk

August 2, 2021

1 Abstract

In this paper we perform for the first time an in-depth analysis of the spectra in the phenomenological supersymmetric Standard Model that simultaneously offer an explanation for the $(g - 2)_\mu$ discrepancy Δa_μ , result in the right dark-matter relic density $\Omega_{\text{DM}} h^2$ and are minimally fine-tuned. The resulting spectra may be obtained from [1]. To discuss the experimental exclusion potential for our models, we analyse the resulting LHC phenomenology as well as the sensitivity of dark-matter direct detection experiments to these spectra. We find that the latter type of experiments with sensitivity to the spin-dependent dark-matter – nucleon scattering cross section $\sigma_{\text{SD,p}}$ will probe all of our found solutions.

10

11 Contents

12	1 Introduction	2
13	2 The muon anomalous magnetic moment and fine-tuning in the pMSSM	3
14	2.1 Electroweak fine-tuning in the pMSSM	4
15	2.2 The muon anomalous magnetic moment	5
16	3 Analysis setup	6
17	4 Phenomenology	6
18	4.1 LHC phenomenology for the funnel regimes	9
19	4.2 LHC phenomenology for the coannihilation regimes	11
20	4.3 LHC phenomenology for the bino-higgsino LSP	12
21	4.4 Dark-matter direct detection experiments	13
22	5 Conclusion	14
23	References	15

24

25

26 1 Introduction

27 The Large Hadron Collider (LHC) has been searching for over a decade for signs of physics
 28 that originate from beyond-the-Standard-Model (BSM) scenarios, including searches for
 29 signals that originate from supersymmetric (SUSY) particle production. These high-energy
 30 searches are complemented by low-energy experiments such as dark-matter (DM) exper-
 31 iments, or experiments that search for small deviations in known Standard-Model (SM)
 32 processes from their SM prediction. In the former category, the XENON1T [2,3], PandaX-
 33 II [4,5] and PICO [6–8] experiments provide limits on the DM-nucleus scattering cross
 34 section, whereas the Planck collaboration provides a precise measurement of the DM relic
 35 abundance [9]. In the latter category, the anomalous magnetic moment of the muon $(g-2)_\mu$
 36 plays an important role. There is a long-standing discrepancy between the experimental
 37 result [10–12] and the SM prediction for the muon anomalous magnetic moment. The
 38 latter is composed of quantum-electrodynamic, weak, hadronic vacuum-polarization, and
 39 hadronic light-by-light contributions, and reads [13–34]

$$a_\mu^{\text{SM}} = \frac{(g-2)_\mu}{2} = 116\,591\,810(43) \times 10^{-11}, \quad (1)$$

40 where the value between parentheses represents the theoretical uncertainty. The improved
 41 experimental results obtained at Fermilab [35–38], combined with the Brookhaven re-
 42 sult [10–12] read

$$a_\mu^{\text{exp}} = 116\,592\,061(41) \times 10^{-11}, \quad (2)$$

43 showing that the deviation is now

$$\Delta a_\mu = a_\mu^{\text{exp}} - a_\mu^{\text{SM}} = 251(59) \times 10^{-11}. \quad (3)$$

44 An independent experiment with different techniques than those employed by the Fermilab
 45 experiment is being constructed at J-PARC [39,40].

46 The Minimal Supersymmetric Standard Model (MSSM) with R -parity conservation pre-
 47 dicta a DM candidate and can simultaneously provide an explanation for the $(g-2)_\mu$
 48 discrepancy¹. Furthermore, the MSSM provides a solution to the fine-tuning (FT) prob-
 49 lem in the Higgs sector that any BSM model introduces, even after taking into account
 50 the constraints on colored sparticles originating from the LHC. It is clear that for a rich
 51 model such as the MSSM, the interplay between the various experimental results is of
 52 crucial importance. In this context, several studies have been performed to study a subset
 53 of these constraints. For instance, the interplay between the LHC limits and the $(g-2)_\mu$
 54 discrepancy has been studied in e.g. Ref. [42–49]. DM direct detection (DMDD) searches
 55 are complementary in regions of the MSSM parameter space where the LHC has little
 56 sensitivity, for example in compressed regions. Papers that explore the DM implications of
 57 spectra that explain the $(g-2)_\mu$ discrepancy include Refs. [48–53], where the relic density
 58 requirement is not always taken into account. Likelihood analyses or global fits, where all
 59 experimental data that constrain the MSSM parameter space are taken into account, have
 60 been performed in e.g. Ref. [53–59]. The degree of FT in constrained models that explain
 61 the $(g-2)_\mu$ discrepancy is studied in [60,61], whereas the role of FT in spectra with the
 62 right DM properties is studied in Ref. [62–66].

63 In this work we perform for the first time a study of the phenomenology of the MSSM
 64 that simultaneously accounts for the DM relic abundance and the observed discrepancy

¹A simultaneous explanation of the muon and electron anomalous magnetic moments in the MSSM context is provided in Ref. [41].

65 of $(g - 2)_\mu$, that includes all DMDD and LHC limits, and that constrains the model-
 66 parameter space to models that are minimally fine-tuned. The resulting spectra may be
 67 obtained from [1]. The paper is structured as follows. In Section 2 we introduce our nota-
 68 tion, the muon anomalous magnetic moment and the electroweak fine-tuning measure. In
 69 Section 3 we explain the set-up of our analysis. In Section 4 we explore the phenomenology
 70 of the viable spectra, and in Section 5 we present our conclusions.

71 2 The muon anomalous magnetic moment and fine-tuning in 72 the pMSSM

73 Instead of exploring the full MSSM with 105 free parameters, we focus on the phenom-
 74 logical MSSM (pMSSM) [67], which has 19 free parameters whose boundary conditions are
 75 given at the SUSY scale of $\mathcal{O}(1 \text{ TeV})$. In this phenomenologically motivated pMSSM one
 76 requires that the first and second generation squark and slepton masses are degenerate,
 77 that the trilinear couplings of the first and second generation sfermions are set to zero
 78 (leaving only those of the third generation, A_t , A_b and A_τ), and that no new sources of
 79 CP violation are introduced. In addition one assumes that all sfermion mass matrices are
 80 diagonal. The sfermion soft-masses are then described by the first and second generation
 81 squark masses $m_{\tilde{Q}_1}$, $m_{\tilde{u}_R}$ and $m_{\tilde{d}_R}$, the third generation squark masses $m_{\tilde{Q}_3}$, $m_{\tilde{t}_R}$ and $m_{\tilde{b}_R}$,
 82 the first and second generation of slepton masses $m_{\tilde{L}_1}$ and $m_{\tilde{e}_R}$, and the third generation
 83 of slepton masses $m_{\tilde{L}_3}$ and $m_{\tilde{\tau}_R}$. The Higgs sector is described by the ratio of the Higgs
 84 vacuum expectation values $\tan \beta$ and the soft Higgs masses m_{H_u} and m_{H_d} . Instead of
 85 these parameters, it is customary to use the higgsino mass parameter μ and the mass m_A
 86 of the pseudoscalar Higgs boson as free parameters. The gaugino sector consists of the
 87 bino (\tilde{B}), wino (\tilde{W}) and gluino with their mass parameters $M_1 (= |M_1|)$, $M_2 (= |M_2|)$ and
 88 $M_3 (= |M_3|)$.

89 As a result of electroweak symmetry breaking (EWSB), the gaugino and the higgsino in-
 90 teraction eigenstates mix into mass eigenstates, called neutralinos and charginos. The
 91 neutralinos, denoted by $\tilde{\chi}_i^0$ with $i = 1, \dots, 4$, are the neutral mass eigenstates of the bino,
 92 wino and higgsino interaction eigenstates. The neutralinos are ordered by increasing mass,
 93 with $\tilde{\chi}_1^0$ the lightest neutralino. Given the constraints from DMDD experiments on sneu-
 94 trino DM, we take the lightest neutralino as lightest-supersymmetric particle (LSP), which
 95 makes it our DM candidate. Depending on the exact values of M_1 , M_2 and $|\mu|$, this lightest
 96 mass eigenstate can be mostly bino-like (if M_1 is smallest), wino-like (if M_2 is smallest)
 97 or higgsino-like (if $|\mu|$ is smallest). The amount of bino, wino and higgsino mixing of the
 98 lightest neutralino is given by N_{11} , N_{12} and $\sqrt{N_{13}^2 + N_{14}^2}$, where N_{ij} are the entries of the
 99 matrix that diagonalizes the neutralino mass matrix. In the basis of $(\tilde{B}, \tilde{W}^0, \tilde{H}_d^0, \tilde{H}_u^0)$, this
 100 mass matrix is given by

$$M_{\tilde{\chi}^0} = \begin{pmatrix} M_1 & 0 & -c_\beta s_{\theta_W} M_Z & s_\beta s_{\theta_W} M_Z \\ 0 & M_2 & c_\beta c_{\theta_W} M_Z & -s_\beta c_{\theta_W} M_Z \\ -c_\beta s_{\theta_W} M_Z & c_\beta c_{\theta_W} M_Z & 0 & -\mu \\ s_\beta s_{\theta_W} M_Z & -s_\beta c_{\theta_W} M_Z & -\mu & 0 \end{pmatrix}, \quad (4)$$

101 with $s_x \equiv \sin x$, $c_x \equiv \cos x$, and the ratio of the SM W - and Z -boson masses being denoted
 102 by $\cos \theta_W = M_W/M_Z$.

103 The charginos, denoted by $\tilde{\chi}_i^\pm$ with $i = 1, 2$, are the charged mass eigenstates of the
 104 wino and higgsino interaction eigenstates, with $\tilde{\chi}_1^\pm$ the lightest chargino. In the basis of

105 $(\widetilde{W}^\pm, \widetilde{H}_{u/d}^\pm)$, their mass matrix at tree level reads

$$M_{\widetilde{\chi}^\pm} = \begin{pmatrix} M_2 & \sqrt{2}c_\beta c_{\theta_W} M_Z \\ \sqrt{2}s_\beta c_{\theta_W} M_Z & \mu \end{pmatrix}. \quad (5)$$

106 The composition of the lightest chargino is predominantly higgsino when $|\mu| < M_2$, pre-
107 dominantly wino when $M_2 < |\mu|$, or a mixture when the two gaugino parameters are close
108 in value.

109 2.1 Electroweak fine-tuning in the pMSSM

110 The EWSB conditions link M_Z to the input parameters via the minimization of the scalar
111 potential of the Higgs fields. The resulting equation at one loop is [68, 69]

$$\frac{M_Z^2}{2} = \frac{m_{H_d}^2 + \Sigma_d^d - (m_{H_u}^2 + \Sigma_u^u) \tan^2 \beta}{\tan^2 \beta - 1} - \mu^2, \quad (6)$$

112 where the two effective potential terms Σ_u^u and Σ_d^d denote the one-loop corrections to
113 the soft SUSY breaking Higgs masses (explicit expressions are shown in the appendix of
114 Ref. [69]). In order to obtain the observed value of $M_Z = 91.2$ GeV, one needs some degree
115 of cancellation between the SUSY parameters appearing in Eq. (6). If small relative changes
116 in the SUSY parameters will result in a distinctly different value of M_Z , the considered
117 spectrum is said to be fine-tuned, as then a large degree of cancellation is needed to obtain
118 the right value of M_Z . FT measures aim to quantify this sensitivity of M_Z to the SUSY
119 input parameters.

120 The electroweak (EW) FT measure [70, 71] is an agnostic approach to the computation of
121 fine-tuning. We take this approach because a generic broken minimal SUSY theory has
122 two relevant energy scales: a high-scale one at which SUSY breaking takes place, and a
123 low-scale one (M_{SUSY}) where the resulting SUSY particle spectrum is situated and the
124 EWSB conditions must be satisfied. We do not know which and how many fundamental
125 parameters exist for a possible high-scale theory. The EW FT measure does not take such
126 underlying high-scale model assumptions into account for its computation. The EW FT
127 measure (Δ_{EW}) parameterizes how sensitive M_Z is to variations in each of the coefficients
128 C_i , which are evaluated at M_Z . It is defined as

$$\Delta_{\text{EW}} \equiv \max_i \left| \frac{C_i}{M_Z^2/2} \right|, \quad (7)$$

129 where the C_i are

$$C_{m_{H_d}} = \frac{m_{H_d}^2}{\tan^2 \beta - 1}, \quad C_{m_{H_u}} = \frac{-m_{H_u}^2 \tan^2 \beta}{\tan^2 \beta - 1}, \quad C_\mu = -\mu^2,$$

$$C_{\Sigma_d^d} = \frac{\max(\Sigma_d^d)}{\tan^2 \beta - 1}, \quad C_{\Sigma_u^u} = \frac{-\max(\Sigma_u^u) \tan^2 \beta}{\tan^2 \beta - 1}.$$

130 The tadpole contributions Σ_u^u and Σ_d^d contain a sum of different contributions. These
131 contributions are computed individually and the maximum contribution is used to compute
132 the $C_{\Sigma_u^u}$ and $C_{\Sigma_d^d}$ coefficients. We will use an upper bound of $\Delta_{\text{EW}} < 100$ (implying no
133 worse than $\mathcal{O}(1\%)$ fine-tuning on the mass of the Z -boson) to determine whether a given
134 set of MSSM parameters is fine-tuned, and use the code from Ref. [64] to compute the
135 measure.

136 Using this measure, one generically finds that minimally fine-tuned scenarios have low

137 values for $|\mu|$, where $\Delta_{\text{EW}} = 100$ is reached at $|\mu| \simeq 800$ GeV [64, 66, 70, 72–76]. The
 138 masses of the gluino, sbottom, stop and squarks are allowed to get large for models with
 139 low Δ_{EW} [65, 77, 78]. Therefore, we assume that the masses of these sparticles are above
 140 2.5 TeV (for the gluino), above 1.2 TeV (for the stops and bottoms) and above 2 TeV (for
 141 the squarks), such that they evade the ATLAS and CMS limits ².

142 2.2 The muon anomalous magnetic moment

143 In the pMSSM, one-loop contributions to a_μ arise from diagrams with a chargino-sneutrino
 144 or neutralino-smuon loop [79]. The expressions for these one-loop corrections read [80]

$$\delta a_\mu^{\tilde{\chi}^0} = \frac{m_\mu}{16\pi^2} \sum_{i=1}^4 \sum_{m=1}^2 \left[-\frac{m_\mu}{12m_{\mu m}^2} (|n_{im}^L|^2 + |n_{im}^R|^2) F_1^N \left(\frac{m_{\tilde{\chi}_i^0}^2}{m_{\mu m}^2} \right) + \frac{m_{\tilde{\chi}_i^0}}{3m_{\mu m}^2} \text{Re} [n_{im}^L n_{im}^R] F_2^N \left(\frac{m_{\tilde{\chi}_i^0}^2}{m_{\mu m}^2} \right) \right], \quad (8)$$

$$\delta a_\mu^{\tilde{\chi}^\pm} = \frac{m_\mu}{16\pi^2} \sum_{k=1}^2 \left[\frac{m_\mu}{12m_{\nu\mu}^2} (|c_k^L|^2 + |c_k^R|^2) F_1^C \left(\frac{m_{\tilde{\chi}_k^\pm}^2}{m_{\nu\mu}^2} \right) + \frac{2m_{\tilde{\chi}_k^\pm}}{3m_{\nu\mu}^2} \text{Re} [c_k^L c_k^R] F_2^C \left(\frac{m_{\tilde{\chi}_k^\pm}^2}{m_{\nu\mu}^2} \right) \right] \quad (9)$$

145 with m_μ the muon mass, $m_{\tilde{\mu}_m}$ the first or second smuon mass, $m_{\tilde{\nu}_\mu}$ the muon sneutrino
 146 mass, i , m and k the indices for the neutralinos, smuons and charginos and the couplings

$$n_{im}^R = \sqrt{2}g_1 N_{i1} X_{m2} + y_\mu N_{i3} X_{m1}, \quad n_{im}^L = \frac{1}{\sqrt{2}} (g_2 N_{i2} + g_1 N_{i1}) X_{m1}^* - y_\mu N_{i3} X_{m2}^* \quad (10)$$

$$c_k^R = y_\mu U_{k2}, \quad c_k^L = -g_2 V_{k1}. \quad (11)$$

147 The down-type muon Yukawa coupling is denoted by $y_\mu = g_2 m_\mu / (\sqrt{2} M_W \cos \beta)$, and the
 148 SU(2) and U(1) gauge couplings are g_2 and g_1 . The matrices N and U , V diagonalize
 149 the neutralino and chargino mass matrices (Eq. (4), (5)), while the unitary matrix X
 150 diagonalizes the smuon mass matrix M_μ^2 , which reads for the pMSSM in the $(\tilde{\mu}_L, \tilde{\mu}_R)$ basis

$$M_\mu^2 = \begin{pmatrix} m_{L_1}^2 + \left(s_{\theta_W}^2 - \frac{1}{2}\right) M_Z^2 \cos(2\beta) & -m_\mu \mu \tan \beta \\ -m_\mu \mu \tan \beta & m_{e_R}^2 - s_{\theta_W}^2 M_Z^2 \cos(2\beta) \end{pmatrix}. \quad (12)$$

152 The loop functions $F_{1,2}^N$ and $F_{1,2}^C$ can be found in Ref. [80]. They are normalized such that
 153 $F_{1,2}^{N,C}(x=1) = 1$, and go to zero for $x \rightarrow \infty$.

154 At two-loop, the numerical values of the various contributions differ considerably. The
 155 photonic Barr-Zee diagrams are the source of the largest possible two-loop contribution.
 156 Here a Higgs boson and a photon connect to either a chargino or sfermion loop [81] ³.

157 As one can see in the expressions above, the chargino-sneutrino and neutralino-smuon
 158 contributions are controlled by M_1 , M_2 , $\tan \beta$ and μ (through $m_{\tilde{\chi}_i^0}$ and $m_{\tilde{\chi}_k^\pm}$), as well as
 159 $m_{\tilde{L}_1}$ and $m_{\tilde{e}_R}$ (through $m_{\tilde{\mu}_m}$ and $m_{\tilde{\nu}_\mu}$). They are enhanced when $\tan \beta$ grows large and
 160 when simultaneously light ($\mathcal{O}(100)$ GeV) neutralinos/charginos and smuons/sneutrinos
 161 exist in the sparticle spectrum. The Barr-Zee diagrams are enhanced by large values of
 162 $\tan \beta$, small values of m_A and large Higgs-sfermion couplings. In general, the one-loop
 163 chargino-sneutrino contribution dominates over the neutralino-slepton contribution [80],

²Note that those limits are shown to be significantly less stringent for MSSM spectra with rich sparticle decays, see e.g. Ref. [59].

³Two-loop corrections from sfermion loops contribute with a few percent here as well, since we assume heavy squark masses [82, 83].

164 unless there is a large smuon left-right mixing induced by a sizable value for μ [84]. These
 165 latter spectra will however result in slightly higher FT values, which is a direct consequence
 166 of a higher value of $|\mu|$.

167 3 Analysis setup

168 To create the SUSY spectra we use SOFTSUSY 4.0 [85], the Higgs mass is calculated using
 169 FeynHiggs 2.14.2 [86–90], and SUSYHIT [91] is used to calculate the decay of the SUSY
 170 and Higgs particles. Vevacious [92–94] is used to check that the models have at least a
 171 meta-stable minimum state that has a lifetime that exceeds that of our universe and that
 172 this state is not color/charge breaking ⁴. We use SUSY-AI [95] and SMODELS [96–100]
 173 to determine the LHC exclusion of a model point. LHC cross sections for sparticle pro-
 174 duction at NLO accuracy are calculated using Prospino [101]. HIGGSBOUNDS 5.1.1 is
 175 used to determine whether the SUSY models satisfy the LEP, Tevatron and LHC Higgs
 176 constraints [102–109]. MICROMEAS 5.2.1 [110–115] is used to compute the DM relic
 177 density ($\Omega_{\text{DM}}h^2$), the present-day velocity-weighted annihilation cross section ($\langle\sigma v\rangle$) and
 178 the spin-dependent and spin-independent dark-matter–nucleon scattering cross sections
 179 ($\sigma_{\text{SD,p}}$ and $\sigma_{\text{SI,p}}$). For DM indirect detection we only consider the limit on $\langle\sigma v\rangle$ stemming
 180 from the observation of gamma rays originating from dwarf galaxies, which we implement
 181 as a hard cut on each of the channels reported on the last page of Ref. [116]. The current
 182 constraints on the dark-matter–nucleon scattering cross sections originating from various
 183 dark matter direct detection (DMDD) experiments are determined via MICROMEAS,
 184 while future projections of constraints are determined via DDALC 2.0.0 [117]. Flavor
 185 observables are computed with SuperIso 4.1 [118, 119]. The muon anomalous magnetic
 186 moment and its theoretical uncertainty is determined including two-loop corrections and
 187 $\tan\beta$ resummation with GM2Calc [82, 120–122].

188 We use the Gaussian particle filter [123] to search the pMSSM parameter space for in-
 189 teresting areas. The lightest SM-like Higgs boson is required to be in the mass range of
 190 $122 \text{ GeV} \leq m_h \leq 128 \text{ GeV}$. Spectra that do not satisfy the LHC bounds on sparticle
 191 masses, branching fractions of B/D -meson decays, the DMDD, or DM indirect detection
 192 bounds are removed. Our spectra are furthermore required to satisfy the LEP limits on
 193 the masses of the charginos, light sleptons and staus ($m_{\tilde{\chi}_1^\pm} > 103.5 \text{ GeV}$, $m_{\tilde{\tau}^\pm} > 90 \text{ GeV}$
 194 and $m_{\tilde{\nu}_\tau^\pm} > 85 \text{ GeV}$) [124, 125], and the constraints on the invisible and total width of the
 195 Z -boson ($\Gamma_{Z,\text{inv}} = 499.0 \pm 1.5 \text{ MeV}$ and $\Gamma_Z = 2.4952 \pm 0.0023 \text{ GeV}$) [126]. The spectra
 196 surviving all constraints are available via [1] ⁵.

197 4 Phenomenology

198 The main experimental constraints on our models that explain the $(g-2)_\mu$ discrepancy
 199 Δa_μ come from DMDD experiments and the LHC. To understand which spectra are still
 200 viable it is crucial to understand the phenomenology of them, since the experimental ex-
 201 clusion power varies depending on the composition of the neutralinos and charginos. In
 202 this section, we therefore take a look at the different scenarios and contributing compo-

⁴These scenarios appear in the $(g-2)_\mu$ context for large $\mu \tan\beta$, see e.g. Ref. [84].

⁵This repository contains both the raw data and a single CSV file that summarizes the SUSY parameters, masses, and the phenomenology explained in Section 3 of all the surviving spectra. Each line in the CSV file corresponds to one particular spectrum, whose name is uniquely specified and corresponds to the names of the directories of the raw data. The contents of the CSV file is further explained in [1].

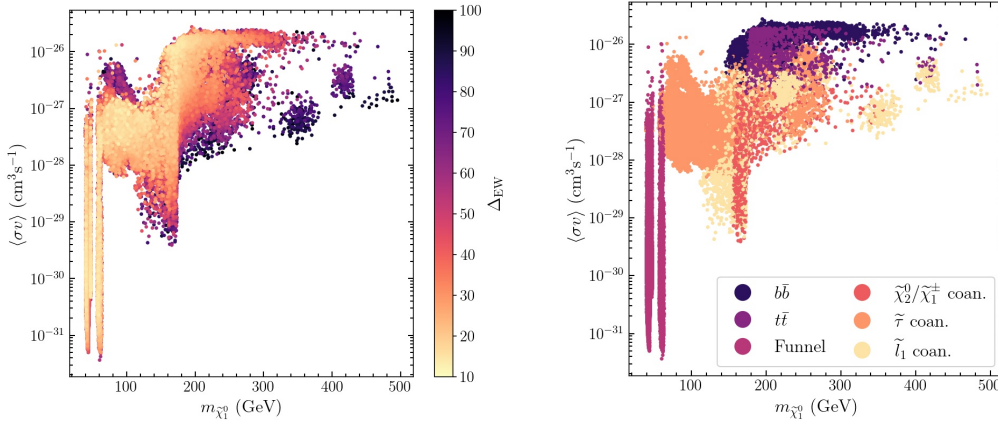


Figure 1: The mass of the DM particle ($m_{\tilde{\chi}_1^0}$) vs the velocity-weighted annihilation cross section ($\langle\sigma v\rangle$). The value of Δ_{EW} is shown as a color code on the left, where the points are ordered such that spectra with lower values of Δ_{EW} lie on top of those with higher values of Δ_{EW} . On the right we show the dominant early-universe annihilation process that contributes to the value of $\Omega_{DM}h^2$. In both plots, we only show points that satisfy all experimental constraints, and have $133 \times 10^{-11} < \Delta a_\mu < 369 \times 10^{-11}$, allowing for a 2σ uncertainty.

203 sitions, and describe in detail the properties of these spectra. Knowing these properties
 204 is also relevant for considering future experimental setups, e.g. for LHC studies where the
 205 exclusion power heavily depends on the assumed model.

206 We first discuss the DM phenomenology of the LSP. We assume that the DM abundance
 207 is determined by thermal freeze-out and require that the lightest neutralino saturates
 208 $\Omega_{DM}h^2$ with the observed value of 0.12 [9] within 0.03 to allow for a theoretical uncer-
 209 tainty on the relic-density calculation. As explained above, the mass eigenstate of the
 210 DM particle is a mixture of bino, wino and higgsino interaction eigenstates. To obtain
 211 the correct relic density in the pMSSM with a pure state, one can either have a higgsino
 212 with a mass of $m_{\tilde{\chi}_1^0} \simeq 800$ GeV or a wino with $m_{\tilde{\chi}_1^0} \simeq 2.5$ TeV. Spectra that saturate the
 213 relic density with lower DM masses necessarily are predominantly bino-like, mixed with
 214 higgsino/wino components. Negligible higgsino/wino components are found in so-called
 215 funnel regions [127, 128], i.e. regions where the mass of the DM particle is roughly half of
 216 the mass of the Z boson, SM-like Higgs boson or heavy Higgs boson. In such a scenario,
 217 the mass of the neutralino can even get below 100 GeV with $M_1 < 100$ GeV, and in par-
 218 ticular the early-universe DM annihilation cross section is enhanced for $m_{\tilde{\chi}_1^0} \simeq m_h/2$ and
 219 $M_Z/2$. Moreover, spectra with another particle close in mass to the LSP can satisfy the
 220 relic density constraint without having a large wino/higgsino component too, due to the
 221 co-annihilation mechanism [129].

222 Requiring that our spectra are simultaneous minimally fine-tuned and satisfy the Δa_μ
 223 constraint removes two types of solutions where the DM relic density constraint is satis-
 224 fied. Firstly, the case where the lightest neutralino is predominantly wino-like results in a
 225 fine-tuned spectrum: to obtain the right relic density $M_2 \simeq 2.5$ TeV for a pure wino, so
 226 $|\mu| > 2.5$ TeV in that scenario. Secondly, the pure-higgsino solutions with the right Ωh^2
 227 do result in $\Delta_{EW} < 100$, but do not allow for an explanation of Δa_μ , which will explicitly
 228 be shown in Section 4.4. Therefore we will see that our solutions feature predominantly
 229 bino-like LSPs. Due to the combined Δa_μ constraint (requiring high $\tan\beta$), DMDD limits
 230 and the FT requirement, the composition has a small higgsino component ($< 20\%$) and a
 231 negligible wino component.

232

233 On the left-hand side of Fig. 1 we show the spectra that survive all constraints and have

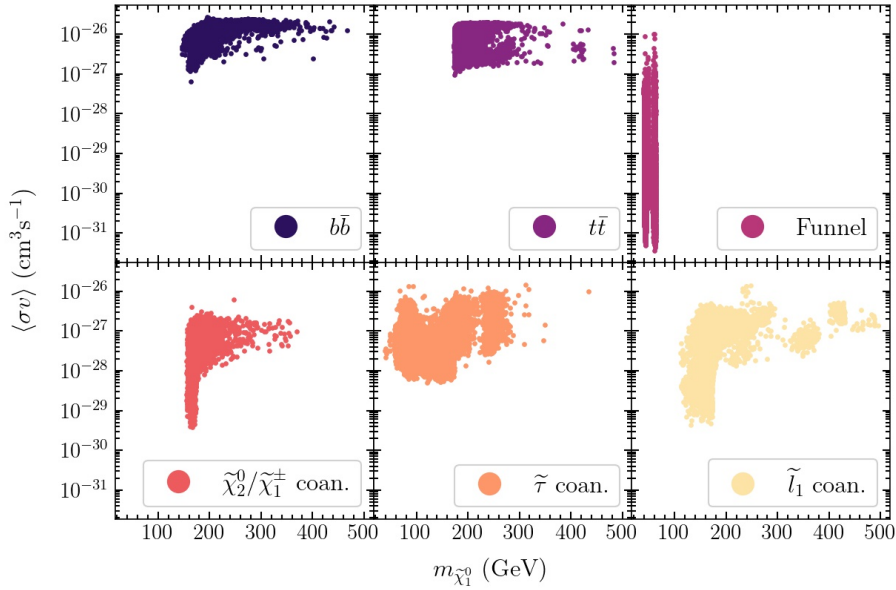


Figure 2: The mass of the DM particle ($m_{\tilde{\chi}_1^0}$) vs the velocity-weighted annihilation cross section ($\langle\sigma v\rangle$). The same points as in Fig. 1 are shown, but split out individually for each early-universe annihilation process.

234 $\Delta_{\text{EW}} < 100$. Lower values for Δ_{EW} are generally found for lower DM masses. The mass
 235 of the DM particle does not exceed 500 GeV, which is a direct result of the combined
 236 requirements of having $\Delta_{\text{EW}} < 100$ and a sufficiently high contribution to Δa_μ . The
 237 lowest-obtained value is $\Delta_{\text{EW}} = 12.3$. From the right-hand side of Fig. 1, we can distinguish
 238 three different type of DM early-universe annihilation mechanisms: the funnel regions, the
 239 coannihilation regions and the bino-higgsino solution (indicated with $b\bar{b}$ and $t\bar{t}$). For clarity
 240 we show in Fig. 2 the same plot split out per annihilation channel, where it clearly can be
 241 seen that for example the $t\bar{t}$ and $b\bar{b}$ annihilation regimes overlap.

242 Before discussing the phenomenology of each of these regions in more detail, we first discuss
 243 the compositions of the LSP, the second-to-lightest neutralino and the lightest chargino.
 244 As anticipated in the previous section, and as shown in Fig. 3, we find that the LSP is
 245 predominantly bino-like and has a small higgsino component. Larger higgsino components
 246 are generally found for spectra that show larger values of $\langle\sigma v\rangle$. The second-to-lightest
 247 neutralino and the lightest chargino are either wino-like, higgsino-like, or mixed wino-
 248 higgsino states. It might be surprising to read that spectra with bino-higgsino LSPs are
 249 allowed to have wino-like $\tilde{\chi}_2^0/\tilde{\chi}_1^\pm$, as one would expect that in general these sparticles would
 250 be predominantly higgsino-like. Such configurations can however be found in spectra for
 251 which M_1 , M_2 and $|\mu|$ are all of $\mathcal{O}(100)$ GeV with M_2 being smaller than $|\mu|$, and that
 252 have moderate to large values of $\tan\beta$ ($10 \lesssim \tan\beta \lesssim 20$). From Eq. (4) one may infer that
 253 for such spectra, little mixing can take place between the bino and wino. This results in
 254 negligible wino components of the LSP, whereas $\tilde{\chi}_1^\pm$ and $\tilde{\chi}_2^0$ can be predominantly wino-
 255 like. Moreover, decreasing $|\mu|$ for such models will not only result in a higher higgsino-
 256 component of the LSP, but counter-intuitively also in a *higher* wino component, while the
 257 wino component of $\tilde{\chi}_1^\pm$ and $\tilde{\chi}_2^0$ then *decreases*. The composition of the $\tilde{\chi}_1^\pm$ and $\tilde{\chi}_2^0$ sparticles
 258 is relevant for the LHC phenomenology, as those spectra where these are predominantly
 259 higgsino-like are typically difficult to probe at the LHC due to low production cross sections
 260 compared to the pure wino $\tilde{\chi}_1^\pm/\tilde{\chi}_2^0$ case.

261 In what follows, we will explore the DM phenomenology of each of these regimes in some
 262 more detail (Section 4.1-4.3). We also discuss their LHC phenomenology, and explain why

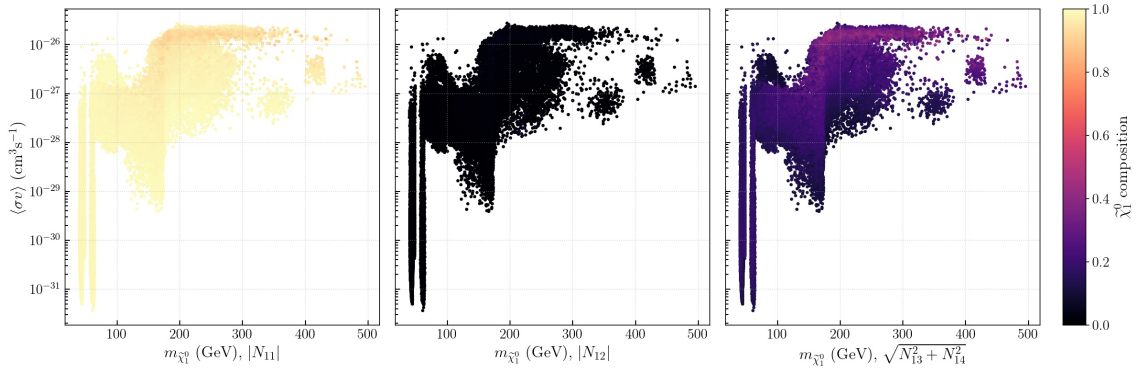


Figure 3: The mass of the DM particle ($m_{\tilde{\chi}_1^0}$) vs the velocity-weighted annihilation cross section ($\langle\sigma v\rangle$). The composition of the LSP is shown as a color code, with the bino component $|N_{11}|$ indicated on the left, the wino component $|N_{12}|$ in the middle, and the higgsino component $\sqrt{N_{13}^2 + N_{14}^2}$ on the right.

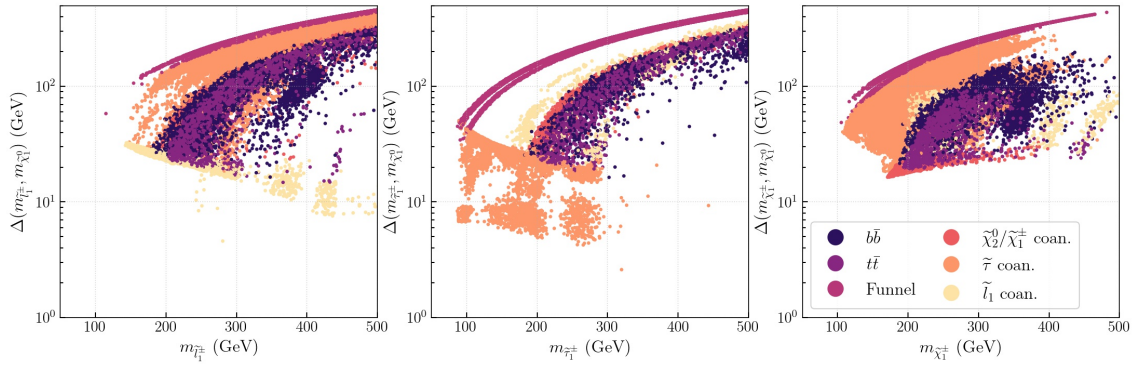


Figure 4: The mass difference between the DM particle and the lightest chargino (left), lightest smuon (middle) and lightest stau (right) versus the mass of the heavier particle. The color code represents the dominant early-universe annihilation channel.

263 our solutions elude the LHC constraints. This allows us to identify gaps in the LHC search
 264 program for supersymmetric particles. We end our discussion on the phenomenology of
 265 the found solutions by discussing the sensitivity of DMDD experiments in Section 4.4.

266 4.1 LHC phenomenology for the funnel regimes

267 We start with discussing the DM phenomenology of the funnel regions, of which there
 268 are two in our spectra ⁶. The first one centers around $m_{\tilde{\chi}_1^0} \simeq 40$ GeV, which is slightly
 269 less than $M_Z/2$. This can be explained as follows. The velocities of the DM particles
 270 were much higher in the early universe than what they are in the present-day universe.
 271 This means that DM annihilations via s-channel Z exchanges could happen on-resonance
 272 in the early universe, whereas in the present-day universe these exchanges only happen
 273 off-resonance. This also explains the fact that the value for $\langle\sigma v\rangle$ is allowed to get orders
 274 of magnitude smaller than the value that one usually expects for a thermal relic (around
 275 $\langle\sigma v\rangle = 3 \cdot 10^{-26} \text{ cm}^3 \text{ s}^{-1}$ for a DM mass of 100 GeV). These models are characterized by small
 276 wino/higgsino components of the LSP - otherwise the early-universe annihilation would be
 277 too efficient, resulting in a too-low value of $\Omega_{\text{DM}} h^2$. The second funnel region is centered
 278 around $m_{\tilde{\chi}_1^0} \simeq 60$ GeV, slightly less than $m_h/2$. These DM particles annihilated in the early
 279 universe predominantly via s-channel SM-like Higgs exchanges. No solutions are found

⁶The heavy Higgs funnel is not identified here, and will be left for future study.

280 for spectra with DM masses in-between the two funnel regions. Here, the wino/higgsino
 281 component necessarily needs to increase to satisfy the $\Omega_{\text{DM}}h^2$ requirement, and these
 282 spectra are excluded by DMDD experiments. The minimal value of Δ_{EW} for these spectra
 283 is 13.2.

284 We now consider the compositions of $\tilde{\chi}_1^0$, $\tilde{\chi}_2^0$ and $\tilde{\chi}_1^\pm$, and identify the mass difference
 285 between the LSP and the next-to-lightest SUSY particles in the funnel regimes, as this is
 286 important to understand the LHC phenomenology of these regions. The two funnel regimes
 287 are characterized by light ($m_{\tilde{\chi}_1^0} < 100$ GeV) bino-like LSPs. The $\tilde{\chi}_1^\pm$ and $\tilde{\chi}_2^0$ are degenerate
 288 in mass. They are wino mixtures for masses around 100 – 200 GeV, while they become
 289 higgsino-like for heavier $\tilde{\chi}_1^\pm / \tilde{\chi}_2^0$ (up to $m_{\tilde{\chi}_1^\pm / \tilde{\chi}_2^0} \simeq 500$ GeV). The mass gap between $\tilde{\chi}_1^0$ and
 290 $\tilde{\chi}_2^0$ or $\tilde{\chi}_1^\pm$ ($\Delta(m_{\tilde{\chi}_2^0}, m_{\tilde{\chi}_1^0})$ or $\Delta(m_{\tilde{\chi}_1^\pm}, m_{\tilde{\chi}_1^0})$) is at least around 50 GeV, and exceeds 100 GeV
 291 for $m_{\tilde{\chi}_1^\pm} \gtrsim 150$ GeV (see Fig. 4, left panel). The masses of the sleptons are heavier than
 292 (at least) the masses of $\tilde{\chi}_2^0$ and $\tilde{\chi}_1^\pm$.

293 Three different sorts of decays for $\tilde{\chi}_2^0$ can be identified that are relevant final-state topologies
 294 for LHC searches:

- 295 1. $\tilde{\chi}_2^0 \rightarrow h\tilde{\chi}_1^0$ when $\Delta(m_{\tilde{\chi}_2^0}, m_{\tilde{\chi}_1^0}) > m_h$,
- 296 2. $\tilde{\chi}_2^0 \rightarrow Z\tilde{\chi}_1^0$ when $\Delta(m_{\tilde{\chi}_2^0}, m_{\tilde{\chi}_1^0}) > M_Z$,
- 297 3. off-shell decays when $\Delta(m_{\tilde{\chi}_2^0}, m_{\tilde{\chi}_1^0}) < M_Z$.

298 For $\tilde{\chi}_1^\pm$, there are only two sorts of decays

- 299 1. $\tilde{\chi}_1^\pm \rightarrow W^\pm\tilde{\chi}_1^0$ when $\Delta(m_{\tilde{\chi}_1^\pm}, m_{\tilde{\chi}_1^0}) > M_W$,
- 300 2. off-shell decays when $\Delta(m_{\tilde{\chi}_1^\pm}, m_{\tilde{\chi}_1^0}) < M_W$.

301 We now determine why our points in the funnel region survive the LHC constraints. Given
 302 that the sleptons in these spectra are heavier than $\tilde{\chi}_2^0$ and $\tilde{\chi}_1^\pm$, searches for $\tilde{\chi}_2^0\tilde{\chi}_1^\pm$ production
 303 with on-shell decays of $\tilde{\chi}_2^0 \rightarrow Z\tilde{\chi}_1^0$, such as those in Ref. [130–133], are most sensitive to
 304 our spectra. However, whenever $\Delta(m_{\tilde{\chi}_2^0}, m_{\tilde{\chi}_1^0}) > m_h$, we find that in our models there
 305 exists a mixture between $\tilde{\chi}_2^0 \rightarrow h\tilde{\chi}_1^0$ and $\tilde{\chi}_2^0 \rightarrow Z\tilde{\chi}_1^0$ decays. This is part of the reason
 306 why our models evade the LHC limits: the sensitivity of the experiments drops when $\tilde{\chi}_2^0$
 307 can decay into the SM-like Higgs boson [131, 134]. A second reason why these spectra
 308 evade the LHC limits is that the simplified limits of the searches mentioned above assume
 309 a wino-like $\tilde{\chi}_2^0\tilde{\chi}_1^\pm$ pair, whereas we deal with mixed wino-higgsino pairs. To interpret the
 310 above-mentioned analyses, we show in the left panel of Fig. 5 the average cross section per
 311 10 by 10 GeV bin for $\tilde{\chi}_2^0\tilde{\chi}_1^\pm$ production. We determined whether a given model point is
 312 excluded by parameterizing the upper bounds on the cross sections as shown in Ref. [132],
 313 Fig. 7 and 8, Ref. [131], Fig. 11 and Ref. [133], Fig. 5 and 6. We find that our cross sections
 314 in the regime where $M_Z < \Delta(m_{\tilde{\chi}_2^0}, m_{\tilde{\chi}_1^0}) < m_h$ do not exceed the 95% confidence level
 315 (CL) limits. We expect this situation to change if more LHC data is collected, making the
 316 LHC sensitive to this part of the funnel parameter space. The models with off-shell decays
 317 are slightly more constrained by the current results of the LHC experiments. Particularly
 318 Ref. [133] excludes some of our spectra in this regime that have $m_{\tilde{\chi}_1^\pm}$ up to 210 GeV and
 319 $\Delta(m_{\tilde{\chi}_2^0}, m_{\tilde{\chi}_1^0}) < 55$ GeV. These spectra are explicitly removed from the plots. The LHC
 320 shows limited sensitivity to the models in the mass range of $55 \text{ GeV} < \Delta(m_{\tilde{\chi}_1^\pm}, m_{\tilde{\chi}_1^0}) < M_Z$.
 321 To gain full sensitivity to the funnel regions, this mass range is an important domain to
 322 cover in the LHC searches.

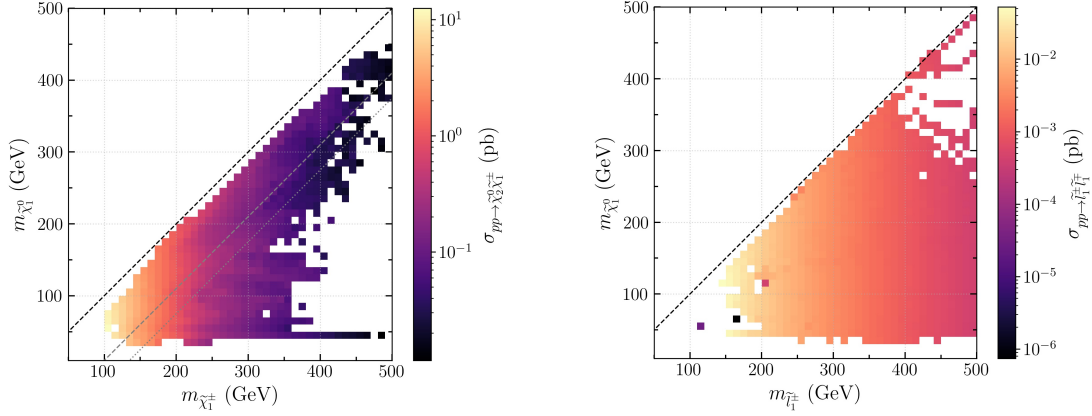


Figure 5: The mass of the DM particle versus the mass of the lightest chargino (left) and smuon (right), combined in 10 by 10 GeV bins. The average production cross section of $\sigma_{pp \rightarrow \tilde{\chi}_2^0 \tilde{\chi}_1^\pm}$ (left) and $\sigma_{pp \rightarrow \tilde{l}_1^\pm \tilde{l}_1^\mp}$ (right) is shown in color code for each bin. The dashed black line in the plot on the left-hand side shows the limit where $m_{\tilde{\chi}_1^0} = m_{\tilde{\chi}_1^\pm}$, whereas the gray dashed (dotted) lines show $m_{\tilde{\chi}_1^\pm} = m_{\tilde{\chi}_1^0} + M_Z$ ($m_{\tilde{\chi}_1^\pm} = m_{\tilde{\chi}_1^0} + m_h$). The dashed black line in the plot on the right-hand side shows $m_{\tilde{\chi}_1^0} = m_{\tilde{l}_1^\pm}$.

323 4.2 LHC phenomenology for the coannihilation regimes

324 The second regime is the coannihilation regime, whose DM phenomenology we now discuss.
 325 It starts to open up at DM masses of roughly 75 GeV, as no charged sparticles (and
 326 therefore no coannihilation partners other than the sneutrino) can exist with masses below
 327 85 GeV due to the LEP/LHC bounds. Three different types of coannihilation partners
 328 are identified: first-/second-generation sleptons, third-generation sleptons, and charginos
 329 or heavier neutralinos. Interestingly, only with the help of slepton coannihilations the
 330 DM particle can have a mass between $\mathcal{O}(70 - 150)$ GeV and still give the right $\Omega_{\text{DM}} h^2$.
 331 To obtain the right relic density in this regime without a slepton-coannihilation partner,
 332 one generally needs high higgsino fractions, which increases the value of $\sigma_{\text{SI,p}}$ beyond
 333 the exclusion limit of the DMDD experiments. The lowest values of Δ_{EW} are found in
 334 the stau-coannihilation regime ($\Delta_{\text{EW}} = 12.3$), while the first-/second-generation slepton
 335 and chargino/neutralino regimes result in lowest values $\Delta_{\text{EW}} = 14.4$ and $\Delta_{\text{EW}} = 16.4$
 336 respectively. The coannihilation regimes are all characterized by small mass differences
 337 between the LSP and its coannihilation partner(s).

338 The first type of coannihilation is that of first-/second-generation sleptons (\tilde{l}_1^\pm). The
 339 compression between $m_{\tilde{l}_1^\pm}$ and $m_{\tilde{\chi}_1^0}$ is increased for higher LSP masses such that the right
 340 $\Omega_{\text{DM}} h^2$ can still be obtained. By computing the production cross section (see Fig. 5),
 341 and comparing these to the results of Fig. 20 of Ref. [134], we see that spectra with
 342 $\Delta(m_{\tilde{\chi}_2^0}, m_{\tilde{\chi}_1^\pm}) > M_Z$ are under strong constraints from searches for $\tilde{\chi}_2^0 \tilde{\chi}_1^\pm \rightarrow \tilde{l} l \nu_l$. We
 343 explicitly remove those points from our data, leaving only models with $\Delta(m_{\tilde{\chi}_2^0}, m_{\tilde{\chi}_1^\pm}) < M_Z$.
 344 The $\tilde{\chi}_1^\pm$ and $\tilde{\chi}_2^0$ sparticles of the surviving models are typically higgsino-like with a small
 345 wino component, and have masses between 180 and 500 GeV.

346 The second coannihilation regime is characterized by low $\tilde{\tau}_1^\pm$ masses. The masses of $\tilde{\chi}_1^\pm/\tilde{\chi}_2^0$
 347 can still be as light as 105 GeV in this regime, where they are predominantly wino-like.
 348 The higgsino component of these particles increases when their masses increase, up to
 349 $m_{\tilde{\chi}_1^\pm/\tilde{\chi}_2^0} \simeq 500$ GeV. Although we have a large production cross section for the wino-like
 350 $\tilde{\chi}_1^\pm/\tilde{\chi}_2^0$ pair, these models are not constrained by the LHC experiments due to the presence
 351 of the light staus. The staus are often lighter than $\tilde{\chi}_1^\pm$ and $\tilde{\chi}_2^0$, and the searches for

352 $\tilde{\tau}_1^\pm$ -mediated decays of $\tilde{\chi}_1^+ \tilde{\chi}_1^- / \tilde{\chi}_1^\pm \tilde{\chi}_2^0$ production have no sensitivity when $\Delta(m_{\tilde{\chi}_1^0}, m_{\tilde{\tau}_1^\pm}) <$
 353 100 GeV [135, 136]. The latter holds for our spectra in the second coannihilation regime,
 354 since the mass differences between the LSP and $\tilde{\tau}_1^\pm$ are between 5 – 50 GeV in that case.
 355 Additionally, relatively few LHC searches for low-mass $\tilde{\tau}^\pm$ particles exist. Small $\tilde{\tau}^+ \tilde{\tau}^-$
 356 production cross sections and low signal acceptances make these searches difficult, so the
 357 experiments have no constraining power in the compressed regime [137, 138]. *We suggest*
 358 *a dedicated low mass $\tilde{\tau}^\pm$ search without an assumed mass degeneracy between $\tilde{\tau}_1^\pm$ and $\tilde{\tau}_2^\pm$*
 359 *to probe the sensitivity of the LHC to these scenarios.*

360 The last coannihilation regime has a $\tilde{\chi}_1^\pm$ or $\tilde{\chi}_2^0$ that is close in mass to the LSP. Interestingly,
 361 although the mass compression for the slepton coannihilation regimes needs to increase to
 362 obtain the right relic density for higher DM masses, for the gaugino-coannihilation regime
 363 it needs to decrease instead. Regarding the LHC phenomenology, note that although the
 364 slepton masses in these regions can be $\mathcal{O}(200)$ GeV, the results from the $\tilde{l}_{R,L}^+ \tilde{l}_{R,L}^-$ searches
 365 with $\tilde{l}^\pm = \tilde{e}^\pm, \tilde{\mu}^\pm$ or $\tilde{\tau}^\pm$ (e.g. [138–140]) are not directly applicable here, as often one or
 366 more of the chargino/heavier neutralino states is lighter than the sleptons. Therefore, the
 367 slepton will not decay with a 100% branching ratio to $\tilde{\chi}_1^0 l^\pm$, although this is assumed
 368 in the above-mentioned searches. Instead, in this regime, only the $\tilde{\chi}_1^\pm \tilde{\chi}_2^0$ searches are of
 369 relevance, similar to the case in the funnel region discussed above. The mass compression
 370 between the LSP and wino-higgsino like $\tilde{\chi}_1^\pm / \tilde{\chi}_2^0$ sparticles is generally around 15–20 GeV,
 371 and Ref. [133] excludes our solutions with $m_{\tilde{\chi}_1^\pm}$ up to 140 – 180 GeV.

372 4.3 LHC phenomenology for the bino-higgsino LSP

373 The last regime we identify consists of bino-higgsino LSPs and is labeled with $b\bar{b}$ and $t\bar{t}$.
 374 These early-universe annihilation channels are mediated by either s-channel Z or h/H ex-
 375 changes. The $t\bar{t}$ annihilation channel opens up when $m_{\tilde{\chi}_1^0}$ becomes larger than the mass
 376 of the top quark m_t , as then the invariant mass of the two LSPs is enough to create a $t\bar{t}$
 377 pair⁷. For the Z -exchange channel this annihilation becomes favored over the annihilation
 378 into a lighter fermion pair, since any Z -mediated annihilation of two Majorana fermions
 379 is helicity suppressed at tree level [141]. This is explained as follows. The two identical
 380 LSPs form a Majorana pair. Such a pair is even under the operation of charge-conjugation
 381 $C = (-1)^{L+S}$ with S the total spin and L the total orbital angular momentum, so L and
 382 S must either both be even, or both be odd. Taking the limit of zero velocity, as the
 383 present-day velocity of DM particles is non-relativistic, we may assume $L = 0$ and even S .
 384 The final-state fermion pair can have a total spin of $S = 1$ or $S = 0$, but only the latter is
 385 allowed for the Majorana-pair annihilation in the non-relativistic limit. For a Dirac-field
 386 pair, an $S = 0$ configuration is obtained if the fermion and anti-fermion are from different
 387 Weyl spinors: a left- and right-handed one. In the SM, a coupling with this combination
 388 only arises (at tree level) by a mass insertion. Therefore, the transition amplitude is pro-
 389 portional to the mass of the final-state fermions, and a decay to a heavier pair of fermions
 390 is generally preferred. In spectra where $\tan\beta$ is large we also see the heavy-Higgs-mediated
 391 decays to $b\bar{b}$, as the bottom-Yukawa coupling is enhanced. As can be seen in Fig. 4, in the
 392 regime of $m_{\tilde{\chi}_1^0} \gtrsim m_t$, the masses of $\tilde{\chi}_1^\pm$ and $\tilde{\chi}_2^0$ are relatively close to that of the LSP, so
 393 due to the coannihilation mechanism these spectra tend to show slightly lower values of
 394 $\langle\sigma v\rangle$ than naively would be expected.

395 The minimal value of Δ_{EW} is around 14.2 for these models. The $\tilde{\chi}_2^0$ and $\tilde{\chi}_1^\pm$ are predomi-
 396 nantly higgsino-like with masses from 180 to 500 GeV. Due to their small production cross
 397 section, the LHC searches do not have exclusion power in this regime.

⁷The annihilation to a W^+W^- pair is possible when $m_{\tilde{\chi}_1^0} > M_W$. However, this is constrained by DMDD due to the high wino/higgsino fraction that is necessary for this channel.

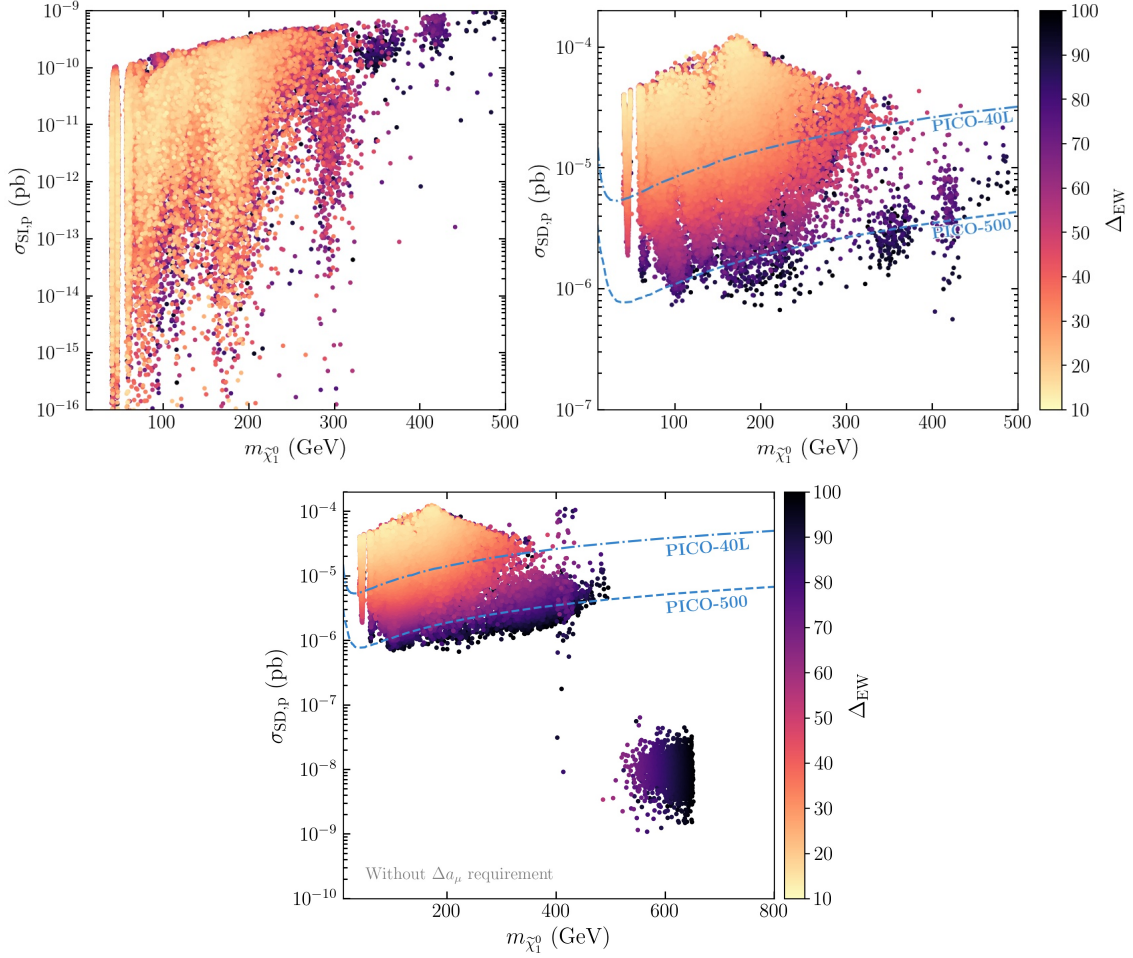


Figure 6: Top right (left): The mass of the DM particle versus the spin-(in)dependent cross section $\sigma_{\text{SD},p}$ ($\sigma_{\text{SI},p}$). The value of Δ_{EW} is shown in color code. We also show the projected PICO-40L and PICO-500 central limits on $\sigma_{\text{SD},p}$ [142]. The points are ordered such that those with lower values of Δ_{EW} lie on top of those with higher values. Bottom: The mass of the DM particle versus $\sigma_{\text{SD},p}$ for spectra satisfying all constraints listed in Section 3 except the Δa_μ requirement. This plot contains the data of the present study combined with that from Ref. [64], where the requirement on a_μ was not taken into account.

398 4.4 Dark-matter direct detection experiments

399 In the previous subsections we discussed the phenomenology of the viable spectra at the
 400 LHC. We now comment on the sensitivity of DMDD experiments. We have seen that the
 401 LSP in our spectra is always bino-like with a small higgsino component (Fig. 3). We find
 402 that the relative size of the wino component of the LSP is constraint by DMDD exper-
 403 iments: higher wino components result in larger values of $\sigma_{\text{SI},p}$ and $\sigma_{\text{SD},p}$. Surprisingly,
 404 this indirectly also places a lower bound on $|\mu|$: decreasing $|\mu|$ for our models will not only
 405 result in a higher higgsino-component, but also in a higher wino component of the LSP, as
 406 more mixing between the wino and bino components is then allowed. Therefore, decreasing
 407 $|\mu|$ for these scenarios is limited by the constraints imposed by the DMDD experiments.
 408 The resulting values for $\sigma_{\text{SI},p}$ and $\sigma_{\text{SD},p}$ of the surviving models may be seen in Fig. 6. While
 409 the value of $\sigma_{\text{SI},p}$ varies by over 7 orders of magnitude, $\sigma_{\text{SD},p}$ is relatively constrained. We
 410 moreover observe that $\sigma_{\text{SD},p}$ is directly correlated with Δ_{EW} : lower values of $\sigma_{\text{SD},p}$
 411 result in higher values of Δ_{EW} . The value of $\sigma_{\text{SD},p}$ decreases with smaller higgsino fractions in
 412 the LSP, while for a given fixed LSP mass Δ_{EW} increases since $|\mu|$ needs to increase. In

413 this figure we also indicate the projected limit of the PICO-40L and the PICO-500 ex-
 414 periments [142]. We observe that the latter one is sensitive to all of our solutions with
 415 $\Delta_{EW} < 62$. The LUX-ZEPLIN experiment [143] (whose projected limit is not shown in
 416 Fig. 6) will probe all of our solutions with $\Delta_{EW} < 100$.
 417 This shows an important message, namely that *future DMDD experiments that probe $\sigma_{SD,p}$*
 418 *will be sensitive to all our solutions, irrespective of the masses and compositions of the rest*
 419 *of the sparticle spectrum*. That the Δa_μ requirement is crucial to obtain this conclusion is
 420 shown in the bottom panel of Fig. 6, where we show both the spectra from this work and
 421 those from Ref. [64] without imposing the Δa_μ constraint. One may observe that in this
 422 case spectra survive with $m_{\tilde{\chi}_1^0} > 500$ GeV that show very small values of $\sigma_{SD,p}$. These pure
 423 higgsino solutions have vanishing couplings to the Z -boson and therefore evade detection
 424 at future DMDD experiments, but do not satisfy the Δa_μ requirement.

425 5 Conclusion

426 In this paper we for the first time have analyzed the spectra in the pMSSM that are min-
 427 imally fine-tuned, result in the right $\Omega_{DM} h^2$ and simultaneously offer an explanation for
 428 Δa_μ . We make these spectra publicly available under [1].

429 In terms of DM phenomenology, we have distinguished three interesting branches of so-
 430 lutions: the funnel regimes, three types of coannihilation regimes, and the generic bino-
 431 higgsino solution. All these solutions have in common that the LSP is predominantly
 432 bino-like with a small higgsino component. Masses of the DM particle range between
 433 39 – 495 GeV. We discussed the phenomenology at the LHC for each of the regimes. The
 434 first and second regime are relatively more constrained by $\tilde{\chi}_2^0 \tilde{\chi}_1^\pm$ searches at the LHC than
 435 the last regime, which is due to the lower wino-components and higher masses of the $\tilde{\chi}_2^0 / \tilde{\chi}_1^\pm$
 436 sparticles that is typical in the last regime. On the other hand, in particular when the
 437 coannihilation partner of the LSP is a light stau, the LHC searches show little to no sen-
 438 sitivity to our found solutions. Our solutions motivate further the ongoing efforts at the
 439 LHC to probe pMSSM spectra that feature (compressed) higgsino-like production of $\tilde{\chi}_2^0 \tilde{\chi}_1^\pm$
 440 pairs. In addition, to increase the sensitivity of the LHC to our found solutions, we find
 441 that a dedicated low-mass $\tilde{\tau}^\pm$ search without an assumed mass degeneracy between $\tilde{\tau}_1^\pm$ and
 442 $\tilde{\tau}_2^\pm$ would be needed, but also that the mass-gap region of $55 \text{ GeV} < \Delta(m_{\tilde{\chi}_2^0}, m_{\tilde{\chi}_1^0}) < M_Z$
 443 is not probed at the LHC. Proposing a dedicated search for these regimes, however, lies
 444 beyond the scope of this work.

445 We find that DMDD experiments that probe $\sigma_{SD,p}$ will ultimately be sensitive to all of
 446 our minimally fine-tuned spectra. The requirement of satisfying Δa_μ is crucial to arrive
 447 at this conclusion. This requirement excludes models with a higher-mass higgsino with
 448 $m_{\tilde{\chi}_1^0} = 550 - 650$ GeV as the LSP, and these spectra would evade detection by future
 449 DMDD experiments.

450 Acknowledgments

451 MvB acknowledges support from the Science and Technology Facilities Council (grant
 452 number ST/T000864/1).

453 **References**

- 454 [1] M. van Beekveld, *Supplementary Data: "Dark matter, fine-tuning and $\mu(g-2)$ in*
455 *the $pMSSM$ "*, doi:10.5281/zenodo.4934398 (2021).
- 456 [2] E. Aprile *et al.*, *Dark matter search results from a one ton-year*
457 *exposure of XENON1T*, Phys. Rev. Lett. **121**(11), 111302 (2018),
458 doi:10.1103/PhysRevLett.121.111302, 1805.12562.
- 459 [3] E. Aprile *et al.*, *Constraining the spin-dependent WIMP-nucleon cross*
460 *sections with XENON1T*, Phys. Rev. Lett. **122**(14), 141301 (2019),
461 doi:10.1103/PhysRevLett.122.141301, 1902.03234.
- 462 [4] J. Xia *et al.*, *PandaX-II constraints on spin-dependent WIMP-nucleon effective*
463 *interactions*, Phys. Lett. **B792**, 193 (2019), doi:10.1016/j.physletb.2019.02.043,
464 1807.01936.
- 465 [5] A. Tan *et al.*, *Dark matter results from first 98.7 days of data from*
466 *the PandaX-II experiment*, Phys. Rev. Lett. **117**(12), 121303 (2016),
467 doi:10.1103/PhysRevLett.117.121303, 1607.07400.
- 468 [6] C. Amole *et al.*, *Dark Matter Search Results from the Complete Exposure of the*
469 *PICO-60 C_3F_8 Bubble Chamber* (2019), 1902.04031.
- 470 [7] C. Amole *et al.*, *Dark Matter Search Results from the PICO-60 C_3F_8 Bubble Cham-*
471 *ber*, Phys. Rev. Lett. **118**(25), 251301 (2017), doi:10.1103/PhysRevLett.118.251301,
472 1702.07666.
- 473 [8] C. Amole *et al.*, *Improved dark matter search results from PICO-2L Run 2*, Phys.
474 Rev. **D93**(6), 061101 (2016), doi:10.1103/PhysRevD.93.061101, 1601.03729.
- 475 [9] N. Aghanim *et al.*, *Planck 2018 results. VI. Cosmological parameters*, Astron. As-
476 trophys. **641**, A6 (2020), doi:10.1051/0004-6361/201833910, 1807.06209.
- 477 [10] G. W. Bennett *et al.*, *Final Report of the Muon E821 Anomalous Mag-*
478 *netic Moment Measurement at BNL*, Phys. Rev. D **73**, 072003 (2006),
479 doi:10.1103/PhysRevD.73.072003, hep-ex/0602035.
- 480 [11] G. W. Bennett *et al.*, *Measurement of the negative muon anomalous*
481 *magnetic moment to 0.7 ppm*, Phys. Rev. Lett. **92**, 161802 (2004),
482 doi:10.1103/PhysRevLett.92.161802, hep-ex/0401008.
- 483 [12] G. W. Bennett *et al.*, *Measurement of the positive muon anomalous magnetic moment*
484 *to 0.7 ppm*, Phys. Rev. Lett. **89**, 101804 (2002), doi:10.1103/PhysRevLett.89.101804,
485 [Erratum: Phys.Rev.Lett. 89, 129903 (2002)], hep-ex/0208001.
- 486 [13] G. Colangelo, M. Hoferichter and P. Stoffer, *Two-pion contribution to hadronic*
487 *vacuum polarization*, JHEP **02**, 006 (2019), doi:10.1007/JHEP02(2019)006, 1810.
488 00007.
- 489 [14] M. Davier, A. Hoecker, B. Malaescu and Z. Zhang, *Reevaluation of the hadronic*
490 *vacuum polarisation contributions to the Standard Model predictions of the muon*
491 *$g - 2$ and $\alpha(m_Z^2)$ using newest hadronic cross-section data*, Eur. Phys. J. C **77**(12),
492 827 (2017), doi:10.1140/epjc/s10052-017-5161-6, 1706.09436.

- 493 [15] A. Keshavarzi, D. Nomura and T. Teubner, *Muon $g-2$ and $\alpha(M_Z^2)$: a new data-based*
494 *analysis*, Phys. Rev. D **97**(11), 114025 (2018), doi:10.1103/PhysRevD.97.114025,
495 1802.02995.
- 496 [16] M. Hoferichter, B.-L. Hoid and B. Kubis, *Three-pion contribution to hadronic vacuum*
497 *polarization*, JHEP **08**, 137 (2019), doi:10.1007/JHEP08(2019)137, 1907.01556.
- 498 [17] A. Kurz, T. Liu, P. Marquard and M. Steinhauser, *Hadronic contribution to the*
499 *muon anomalous magnetic moment to next-to-next-to-leading order*, Phys. Lett. B
500 **734**, 144 (2014), doi:10.1016/j.physletb.2014.05.043, 1403.6400.
- 501 [18] K. Melnikov and A. Vainshtein, *Hadronic light-by-light scattering contribution to*
502 *the muon anomalous magnetic moment revisited*, Phys. Rev. D **70**, 113006 (2004),
503 doi:10.1103/PhysRevD.70.113006, hep-ph/0312226.
- 504 [19] G. Colangelo, M. Hoferichter, M. Procura and P. Stoffer, *Dispersion relation for*
505 *hadronic light-by-light scattering: two-pion contributions*, JHEP **04**, 161 (2017),
506 doi:10.1007/JHEP04(2017)161, 1702.07347.
- 507 [20] M. Hoferichter, B.-L. Hoid, B. Kubis, S. Leupold and S. P. Schneider, *Disper-*
508 *sion relation for hadronic light-by-light scattering: pion pole*, JHEP **10**, 141 (2018),
509 doi:10.1007/JHEP10(2018)141, 1808.04823.
- 510 [21] A. Gérardin, H. B. Meyer and A. Nyffeler, *Lattice calculation of the pion transition*
511 *form factor with $N_f = 2 + 1$ Wilson quarks*, Phys. Rev. D **100**(3), 034520 (2019),
512 doi:10.1103/PhysRevD.100.034520, 1903.09471.
- 513 [22] G. Colangelo, F. Hagelstein, M. Hoferichter, L. Laub and P. Stoffer, *Longitudinal*
514 *short-distance constraints for the hadronic light-by-light contribution to $(g-2)_\mu$ with*
515 *large- N_c Regge models*, JHEP **03**, 101 (2020), doi:10.1007/JHEP03(2020)101, 1910.
516 13432.
- 517 [23] G. Colangelo, M. Hoferichter, A. Nyffeler, M. Passera and P. Stoffer, *Remarks on*
518 *higher-order hadronic corrections to the muon $g-2$* , Phys. Lett. B **735**, 90 (2014),
519 doi:10.1016/j.physletb.2014.06.012, 1403.7512.
- 520 [24] P. Masjuan and P. Sanchez-Puertas, *Pseudoscalar-pole contribution to the*
521 *$(g_\mu - 2)$: a rational approach*, Phys. Rev. D **95**(5), 054026 (2017),
522 doi:10.1103/PhysRevD.95.054026, 1701.05829.
- 523 [25] T. Blum, N. Christ, M. Hayakawa, T. Izubuchi, L. Jin, C. Jung and C. Lehner,
524 *Hadronic Light-by-Light Scattering Contribution to the Muon Anomalous Mag-*
525 *netic Moment from Lattice QCD*, Phys. Rev. Lett. **124**(13), 132002 (2020),
526 doi:10.1103/PhysRevLett.124.132002, 1911.08123.
- 527 [26] J. Prades, E. de Rafael and A. Vainshtein, *The Hadronic Light-by-Light Scattering*
528 *Contribution to the Muon and Electron Anomalous Magnetic Moments*, Adv. Ser.
529 Direct. High Energy Phys. **20**, 303 (2009), doi:10.1142/9789814271844_0009, 0901.
530 0306.
- 531 [27] M. Davier, A. Hoecker, B. Malaescu and Z. Zhang, *A new evaluation of the hadronic*
532 *vacuum polarisation contributions to the muon anomalous magnetic moment and to*
533 *$\alpha(m_Z^2)$* , Eur. Phys. J. C **80**(3), 241 (2020), doi:10.1140/epjc/s10052-020-7792-2,
534 [Erratum: Eur.Phys.J.C 80, 410 (2020)], 1908.00921.

- 535 [28] A. Keshavarzi, D. Nomura and T. Teubner, *$g - 2$ of charged leptons, $\alpha(M_Z^2)$*
536 *, and the hyperfine splitting of muonium*, Phys. Rev. D **101**(1), 014029 (2020),
537 doi:10.1103/PhysRevD.101.014029, 1911.00367.
- 538 [29] C. Gnendiger, D. Stöckinger and H. Stöckinger-Kim, *The electroweak contributions*
539 *to $(g-2)_\mu$ after the Higgs boson mass measurement*, Phys. Rev. D **88**, 053005 (2013),
540 doi:10.1103/PhysRevD.88.053005, 1306.5546.
- 541 [30] A. Czarnecki, W. J. Marciano and A. Vainshtein, *Refinements in electroweak con-*
542 *tributions to the muon anomalous magnetic moment*, Phys. Rev. D **67**, 073006
543 (2003), doi:10.1103/PhysRevD.67.073006, [Erratum: Phys.Rev.D 73, 119901 (2006)],
544 hep-ph/0212229.
- 545 [31] M. Knecht, S. Peris, M. Perrottet and E. De Rafael, *Electroweak hadronic contribu-*
546 *tions to the muon $(g-2)$* , JHEP **11**, 003 (2002), doi:10.1088/1126-6708/2002/11/003,
547 hep-ph/0205102.
- 548 [32] T. Aoyama, T. Kinoshita and M. Nio, *Revised and Improved Value of the QED*
549 *Tenth-Order Electron Anomalous Magnetic Moment*, Phys. Rev. D **97**(3), 036001
550 (2018), doi:10.1103/PhysRevD.97.036001, 1712.06060.
- 551 [33] T. Aoyama, M. Hayakawa, T. Kinoshita and M. Nio, *Complete Tenth-Order*
552 *QED Contribution to the Muon $g-2$* , Phys. Rev. Lett. **109**, 111808 (2012),
553 doi:10.1103/PhysRevLett.109.111808, 1205.5370.
- 554 [34] T. Aoyama *et al.*, *The anomalous magnetic moment of the muon in the Standard*
555 *Model*, Phys. Rept. **887**, 1 (2020), doi:10.1016/j.physrep.2020.07.006, 2006.04822.
- 556 [35] **Muon $g - 2$ Collaboration**, *Muon $(g-2)$ Technical Design Report* (2015), 1501.
557 06858.
- 558 [36] **Muon $g - 2$ Collaboration**, *Measurement of the positive muon anoma-*
559 *lous magnetic moment to 0.46 ppm*, Phys. Rev. Lett. **126**, 141801 (2021),
560 doi:10.1103/PhysRevLett.126.141801.
- 561 [37] **Muon $g - 2$ Collaboration**, *Magnetic-field measurement and analysis for the*
562 *muon $g - 2$ experiment at fermilab*, Phys. Rev. A **103**, 042208 (2021),
563 doi:10.1103/PhysRevA.103.042208.
- 564 [38] **Muon $g - 2$ Collaboration**, *Measurement of the anomalous precession frequency of*
565 *the muon in the fermilab muon $g - 2$ experiment*, Phys. Rev. D **103**, 072002 (2021),
566 doi:10.1103/PhysRevA.103.042208.
- 567 [39] T. Mibe, *Measurement of muon $g-2$ and edm with an ultra-cold muon beam*
568 *at j -parc*, Nuclear Physics B - Proceedings Supplements **218**(1), 242 (2011),
569 doi:https://doi.org/10.1016/j.nuclphysbps.2011.06.039, Proceedings of the Eleventh
570 International Workshop on Tau Lepton Physics.
- 571 [40] M. Abe *et al.*, *A New Approach for Measuring the Muon Anomalous Mag-*
572 *netic Moment and Electric Dipole Moment*, PTEP **2019**(5), 053C02 (2019),
573 doi:10.1093/ptep/ptz030, 1901.03047.
- 574 [41] M. Badziak and K. Sakurai, *Explanation of electron and muon $g - 2$ anomalies in*
575 *the MSSM*, JHEP **10**, 024 (2019), doi:10.1007/JHEP10(2019)024, 1908.03607.

- 576 [42] K. Kowalska, L. Roszkowski, E. M. Sessolo and A. J. Williams, *GUT-inspired SUSY*
577 *and the muon $g - 2$ anomaly: prospects for LHC 14 TeV*, JHEP **06**, 020 (2015),
578 doi:10.1007/JHEP06(2015)020, 1503.08219.
- 579 [43] M. A. Ajaib, B. Dutta, T. Ghosh, I. Gogoladze and Q. Shafi, *Neutralinos and*
580 *sleptons at the LHC in light of muon $(g - 2)_\mu$* , Phys. Rev. D **92**(7), 075033 (2015),
581 doi:10.1103/PhysRevD.92.075033, 1505.05896.
- 582 [44] S. P. Das, M. Guchait and D. P. Roy, *Testing SUSY models for the muon $g-2$*
583 *anomaly via chargino-neutralino pair production at the LHC*, Phys. Rev. D **90**(5),
584 055011 (2014), doi:10.1103/PhysRevD.90.055011, 1406.6925.
- 585 [45] M. Endo, K. Hamaguchi, S. Iwamoto and T. Kitahara, *Muon $g - 2$ vs LHC Run*
586 *2 in supersymmetric models*, JHEP **04**, 165 (2020), doi:10.1007/JHEP04(2020)165,
587 2001.11025.
- 588 [46] K. Hagiwara, K. Ma and S. Mukhopadhyay, *Closing in on the chargino contribution*
589 *to the muon $g-2$ in the MSSM: current LHC constraints*, Phys. Rev. D **97**(5), 055035
590 (2018), doi:10.1103/PhysRevD.97.055035, 1706.09313.
- 591 [47] H. M. Tran and H. T. Nguyen, *GUT-inspired MSSM in light of muon $g -$*
592 *2 and LHC results at $\sqrt{s} = 13$ TeV*, Phys. Rev. D **99**(3), 035040 (2019),
593 doi:10.1103/PhysRevD.99.035040, 1812.11757.
- 594 [48] M. Abdughani, K.-I. Hikasa, L. Wu, J. M. Yang and J. Zhao, *Testing electroweak*
595 *SUSY for muon $g - 2$ and dark matter at the LHC and beyond*, JHEP **11**, 095
596 (2019), doi:10.1007/JHEP11(2019)095, 1909.07792.
- 597 [49] A. Kobakhidze, M. Talia and L. Wu, *Probing the MSSM explanation of the muon*
598 *$g-2$ anomaly in dark matter experiments and at a 100 TeV pp collider*, Phys. Rev. D
599 **95**(5), 055023 (2017), doi:10.1103/PhysRevD.95.055023, 1608.03641.
- 600 [50] M. Endo, K. Hamaguchi, S. Iwamoto and K. Yanagi, *Probing minimal SUSY*
601 *scenarios in the light of muon $g - 2$ and dark matter*, JHEP **06**, 031 (2017),
602 doi:10.1007/JHEP06(2017)031, 1704.05287.
- 603 [51] M. Chakraborti, S. Heinemeyer and I. Saha, *Improved $(g - 2)_\mu$ Measurements and*
604 *Supersymmetry*, Eur. Phys. J. C **80**(10), 984 (2020), doi:10.1140/epjc/s10052-020-
605 08504-8, 2006.15157.
- 606 [52] P. Cox, C. Han and T. T. Yanagida, *Muon $g - 2$ and dark matter in the*
607 *minimal supersymmetric standard model*, Phys. Rev. D **98**(5), 055015 (2018),
608 doi:10.1103/PhysRevD.98.055015, 1805.02802.
- 609 [53] M. Chakraborti, S. Heinemeyer and I. Saha, *Improved $(g - 2)_\mu$ Measurements and*
610 *Wino/Higgsino Dark Matter* (2021), 2103.13403.
- 611 [54] E. A. Bagnaschi *et al.*, *Supersymmetric Dark Matter after LHC Run 1*, Eur. Phys.
612 J. C **75**, 500 (2015), doi:10.1140/epjc/s10052-015-3718-9, 1508.01173.
- 613 [55] G. Bertone, F. Calore, S. Caron, R. Ruiz, J. S. Kim, R. Trotta and C. Weniger,
614 *Global analysis of the p MSSM in light of the Fermi GeV excess: prospects for the*
615 *LHC Run-II and astroparticle experiments*, JCAP **04**, 037 (2016), doi:10.1088/1475-
616 7516/2016/04/037, 1507.07008.

- 617 [56] C. Streye, G. Bertone, G. J. Besjes, S. Caron, R. Ruiz de Austri, A. Strubig and
618 R. Trotta, *Profile likelihood maps of a 15-dimensional MSSM*, JHEP **09**, 081 (2014),
619 doi:10.1007/JHEP09(2014)081, 1405.0622.
- 620 [57] A. Fowlie, K. Kowalska, L. Roszkowski, E. M. Sessolo and Y.-L. S. Tsai, *Dark
621 matter and collider signatures of the MSSM*, Phys. Rev. D **88**, 055012 (2013),
622 doi:10.1103/PhysRevD.88.055012, 1306.1567.
- 623 [58] E. Bagnaschi *et al.*, *Likelihood Analysis of the p MSSM11 in Light of LHC 13-TeV
624 Data*, Eur. Phys. J. C **78**(3), 256 (2018), doi:10.1140/epjc/s10052-018-5697-0, 1710.
625 11091.
- 626 [59] P. Athron *et al.*, *A global fit of the MSSM with GAMBIT*, Eur. Phys. J. C **77**(12),
627 879 (2017), doi:10.1140/epjc/s10052-017-5196-8, 1705.07917.
- 628 [60] T. Li and S. Raza, *Electroweak supersymmetry from the generalized mini-
629 mal supergravity model in the MSSM*, Phys. Rev. D **91**(5), 055016 (2015),
630 doi:10.1103/PhysRevD.91.055016, 1409.3930.
- 631 [61] T. Li, S. Raza and K. Wang, *Constraining Natural SUSY via the Higgs Coupling and
632 the Muon Anomalous Magnetic Moment Measurements*, Phys. Rev. D **93**(5), 055040
633 (2016), doi:10.1103/PhysRevD.93.055040, 1601.00178.
- 634 [62] M. Drees and G. Ghaffari, *Impact of the Bounds on the Direct Search for Neutralino
635 Dark Matter on Naturalness* (2021), 2103.15617.
- 636 [63] M. Abdughani, L. Wu and J. M. Yang, *Status and prospects of light
637 bino-higgsino dark matter in natural SUSY*, Eur. Phys. J. C **78**(1), 4 (2018),
638 doi:10.1140/epjc/s10052-017-5485-2, 1705.09164.
- 639 [64] M. van Beekveld, W. Beenakker, S. Caron, R. Peeters and R. Ruiz de Austri, *Su-
640 persymmetry with dark matter is still natural*, Phys. Rev. D **96**(3), 035015 (2017),
641 doi:10.1103/PhysRevD.96.035015, 1612.06333.
- 642 [65] M. van Beekveld, S. Caron and R. Ruiz de Austri, *The current status of fine-tuning in
643 supersymmetry*, JHEP **01**, 147 (2020), doi:10.1007/JHEP01(2020)147, 1906.10706.
- 644 [66] H. Baer, V. Barger, D. Sengupta and X. Tata, *Is natural higgsino-only dark matter
645 excluded?*, Eur. Phys. J. C **78**(10), 838 (2018), doi:10.1140/epjc/s10052-018-6306-y,
646 1803.11210.
- 647 [67] **MSSM Working Group**, *The minimal supersymmetric standard model: group
648 summary report*, In *GDR (Groupement De Recherche) - Supersymetrie Montpellier,
649 France, April 15-17, 1998* (1998), 9901246.
- 650 [68] S. R. Coleman and E. J. Weinberg, *Radiative corrections as the origin of spontaneous
651 symmetry breaking*, Phys. Rev. D **7**, 1888 (1973), doi:10.1103/PhysRevD.7.1888.
- 652 [69] H. Baer, V. Barger, P. Huang, D. Mickelson, A. Mustafayev and X. Tata, *Ra-
653 diative natural supersymmetry: Reconciling electroweak fine-tuning and the Higgs
654 boson mass*, Phys. Rev. D **87**(11), 115028 (2013), doi:10.1103/PhysRevD.87.115028,
655 1212.2655.
- 656 [70] H. Baer, V. Barger, P. Huang, A. Mustafayev and X. Tata, *Radiative natural su-
657 persymmetry with a 125 GeV Higgs boson*, Phys. Rev. Lett. **109**, 161802 (2012),
658 doi:10.1103/PhysRevLett.109.161802, 1207.3343.

- 659 [71] H. Baer, V. Barger and D. Mickelson, *How conventional measures overestimate*
660 *electroweak fine-tuning in supersymmetric theory*, Phys. Rev. **D88**(9), 095013 (2013),
661 doi:10.1103/PhysRevD.88.095013, 1309.2984.
- 662 [72] H. Baer, V. Barger and M. Padeffke-Kirkland, *Electroweak versus high scale*
663 *finetuning in the 19-parameter SUGRA model*, Phys. Rev. **D88**, 055026 (2013),
664 doi:10.1103/PhysRevD.88.055026, 1304.6732.
- 665 [73] H. Baer, V. Barger, D. Mickelson and M. Padeffke-Kirkland, *SUSY models under*
666 *siege: LHC constraints and electroweak fine-tuning*, Phys. Rev. **D89**(11), 115019
667 (2014), doi:10.1103/PhysRevD.89.115019, 1404.2277.
- 668 [74] M. Drees and J. S. Kim, *Minimal natural supersymmetry after the LHC8*, Phys.
669 Rev. **D93**(9), 095005 (2016), doi:10.1103/PhysRevD.93.095005, 1511.04461.
- 670 [75] H. Baer, V. Barger, J. S. Gainer, H. Serce and X. Tata, *Reach of the high-energy*
671 *LHC for gluinos and top squarks in SUSY models with light Higgsinos*, Phys. Rev.
672 **D96**(11), 115008 (2017), doi:10.1103/PhysRevD.96.115008, 1708.09054.
- 673 [76] A. Mustafayev and X. Tata, *Supersymmetry, Naturalness, and Light Higgsinos*,
674 Indian J. Phys. **88**, 991 (2014), doi:10.1007/s12648-014-0504-8, 1404.1386.
- 675 [77] H. Baer, V. Barger, P. Huang, D. Mickelson, A. Mustafayev and X. Tata, *Radiative*
676 *natural supersymmetry: Reconciling electroweak fine-tuning and the higgs boson mass*,
677 Phys. Rev. D **87**, 115028 (2013), doi:10.1103/PhysRevD.87.115028.
- 678 [78] H. Baer, V. Barger and M. Savoy, *Upper bounds on sparticle masses from naturalness*
679 *or how to disprove weak scale supersymmetry*, Phys. Rev. D **93**, 035016 (2016),
680 doi:10.1103/PhysRevD.93.035016.
- 681 [79] T. Moroi, *The Muon anomalous magnetic dipole moment in the min-*
682 *imal supersymmetric standard model*, Phys. Rev. D **53**, 6565 (1996),
683 doi:10.1103/PhysRevD.53.6565, [Erratum: Phys.Rev.D 56, 4424 (1997)], hep-ph/
684 9512396.
- 685 [80] S. P. Martin and J. D. Wells, *Muon Anomalous Magnetic Dipole Mo-*
686 *ment in Supersymmetric Theories*, Phys. Rev. D **64**, 035003 (2001),
687 doi:10.1103/PhysRevD.64.035003, hep-ph/0103067.
- 688 [81] D. Stockinger, *The Muon Magnetic Moment and Supersymmetry*, J. Phys. G **34**,
689 R45 (2007), doi:10.1088/0954-3899/34/2/R01, hep-ph/0609168.
- 690 [82] H. Fargnoli, C. Gnendiger, S. Paßehr, D. Stöckinger and H. Stöckinger-Kim, *Two-*
691 *loop corrections to the muon magnetic moment from fermion/sfermion loops in the*
692 *MSSM: detailed results*, JHEP **02**, 070 (2014), doi:10.1007/JHEP02(2014)070, 1311.
693 1775.
- 694 [83] H. G. Fargnoli, C. Gnendiger, S. Paßehr, D. Stöckinger and H. Stöckinger-Kim, *Non-*
695 *decoupling two-loop corrections to $(g-2)_\mu$ from fermion/sfermion loops in the MSSM*,
696 Phys. Lett. B **726**, 717 (2013), doi:10.1016/j.physletb.2013.09.034, 1309.0980.
- 697 [84] M. Endo, K. Hamaguchi, T. Kitahara and T. Yoshinaga, *Probing Bino contribution*
698 *to muon $g-2$* , JHEP **11**, 013 (2013), doi:10.1007/JHEP11(2013)013, 1309.3065.

- 699 [85] B. C. Allanach, *SOFTSUSY: a program for calculating supersymmetric spectra*,
700 Comput. Phys. Commun. **143**, 305 (2002), doi:10.1016/S0010-4655(01)00460-X,
701 hep-ph/0104145.
- 702 [86] H. Bahl and W. Hollik, *Precise prediction for the light MSSM Higgs boson mass*
703 *combining effective field theory and fixed-order calculations*, Eur. Phys. J. **C76**(9),
704 499 (2016), doi:10.1140/epjc/s10052-016-4354-8, 1608.01880.
- 705 [87] T. Hahn, S. Heinemeyer, W. Hollik, H. Rzehak and G. Weiglein, *High-*
706 *precision predictions for the Light CP-even Higgs boson mass of the Minimal*
707 *Supersymmetric Standard Model*, Phys. Rev. Lett. **112**(14), 141801 (2014),
708 doi:10.1103/PhysRevLett.112.141801, 1312.4937.
- 709 [88] M. Frank, T. Hahn, S. Heinemeyer, W. Hollik, H. Rzehak and G. Weiglein, *The*
710 *Higgs boson masses and mixings of the complex MSSM in the Feynman-diagrammatic*
711 *approach*, JHEP **0702**, 047 (2007), doi:10.1088/1126-6708/2007/02/047, 0611326.
- 712 [89] G. Degrandi, S. Heinemeyer, W. Hollik, P. Slavich and G. Weiglein, *Towards high*
713 *precision predictions for the MSSM Higgs sector*, Eur. Phys. J. **C28**, 133 (2003),
714 doi:10.1140/epjc/s2003-01152-2, 0212020.
- 715 [90] S. Heinemeyer, W. Hollik and G. Weiglein, *FeynHiggs: A program for the calculation*
716 *of the masses of the neutral CP even Higgs bosons in the MSSM*, Comput. Phys.
717 Commun. **124**, 76 (2000), doi:10.1016/S0010-4655(99)00364-1, 9812320.
- 718 [91] A. Djouadi, M. M. Muhlleitner and M. Spira, *Decays of supersymmetric particles: the*
719 *program SUSY-HIT (SUspect-SdecaY-Hdecay-InTerface)*, Acta Phys. Polon. **B38**,
720 635 (2007), hep-ph/0609292.
- 721 [92] J. E. Camargo-Molina, B. O’Leary, W. Porod and F. Staub, *Vevacious: A tool*
722 *for finding the global minima of one-loop effective potentials with many scalars*, Eur.
723 Phys. J. **C73**(10), 2588 (2013), doi:10.1140/epjc/s10052-013-2588-2, 1307.1477.
- 724 [93] T. L. Lee, T. Y. Li and C. H. Tsai, *Hom4ps-2.0: a software package for solving*
725 *polynomial systems by the polyhedral homotopy continuation method*, Computing
726 **83**(2), 109 (2008), doi:10.1007/s00607-008-0015-6.
- 727 [94] C. L. Wainwright, *CosmoTransitions: Computing cosmological phase transition tem-*
728 *peratures and bubble profiles with multiple fields*, Comput. Phys. Commun. **183**, 2006
729 (2012), doi:10.1016/j.cpc.2012.04.004, 1109.4189.
- 730 [95] S. Caron, J. S. Kim, K. Rolbiecki, R. Ruiz de Austri and B. Stienen, *The BSM-AI*
731 *project: SUSY-AI-generalizing LHC limits on supersymmetry with machine learning*,
732 Eur. Phys. J. **C77**(4), 257 (2017), doi:10.1140/epjc/s10052-017-4814-9, 1605.02797.
- 733 [96] F. Ambrogio *et al.*, *SModelS v1.2: long-lived particles, combination of signal regions,*
734 *and other novelties* (2018), 1811.10624.
- 735 [97] J. Heisig, S. Kraml and A. Lessa, *Constraining new physics with searches for*
736 *long-lived particles: implementation into SModelS*, Phys. Lett. **B788**, 87 (2019),
737 doi:10.1016/j.physletb.2018.10.049, 1808.05229.
- 738 [98] J. Dutta, S. Kraml, A. Lessa and W. Waltenberger, *SModelS extension with*
739 *the CMS supersymmetry search results from Run 2*, LHEP **1**(1), 5 (2018),
740 doi:10.31526/LHEP.1.2018.02, 1803.02204.

- 741 [99] F. Ambroggi, S. Kraml, S. Kulkarni, U. Laa, A. Lessa, V. Magerl, J. Sonneveld,
742 M. Traub and W. Waltenberger, *SModelS v1.1 user manual: Improving simplified*
743 *model constraints with efficiency maps*, Comput. Phys. Commun. **227**, 72 (2018),
744 doi:10.1016/j.cpc.2018.02.007, 1701.06586.
- 745 [100] S. Kraml, S. Kulkarni, U. Laa, A. Lessa, W. Magerl, D. Proschofsky-Spindler and
746 W. Waltenberger, *SModelS: a tool for interpreting simplified-model results from*
747 *the LHC and its application to supersymmetry*, Eur. Phys. J. **C74**, 2868 (2014),
748 doi:10.1140/epjc/s10052-014-2868-5, 1312.4175.
- 749 [101] W. Beenakker, R. Hopker and M. Spira, *PROSPINO: A Program for the production*
750 *of supersymmetric particles in next-to-leading order QCD* (1996), hep-ph/9611232.
- 751 [102] P. Bechtle, S. Heinemeyer, O. Stål, T. Stefaniak and G. Weiglein, *Applying exclusion*
752 *likelihoods from LHC searches to extended Higgs sectors*, Eur. Phys. J. **C75**(9), 421
753 (2015), doi:10.1140/epjc/s10052-015-3650-z, 1507.06706.
- 754 [103] P. Bechtle, O. Brein, S. Heinemeyer, O. Stål, T. Stefaniak, G. Weiglein and K. E.
755 Williams, *HiggsBounds–4: Improved tests of extended Higgs sectors against exclusion*
756 *bounds from LEP, the Tevatron and the LHC*, Eur. Phys. J. **C74**(3), 2693 (2014),
757 doi:10.1140/epjc/s10052-013-2693-2, 1311.0055.
- 758 [104] P. Bechtle, O. Brein, S. Heinemeyer, O. Stål, T. Stefaniak, G. Weiglein and
759 K. Williams, *Recent developments in HiggsBounds and a preview of HiggsSignals*,
760 PoS **2012**, 024 (2012), doi:10.22323/1.156.0024, 1301.2345.
- 761 [105] P. Bechtle, O. Brein, S. Heinemeyer, G. Weiglein and K. E. Williams, *Higgs-*
762 *Bounds 2.0.0: Confronting neutral and charged Higgs sector predictions with ex-*
763 *clusion bounds from LEP and the Tevatron*, Comput. Phys. Commun. **182**, 2605
764 (2011), doi:10.1016/j.cpc.2011.07.015, 1102.1898.
- 765 [106] P. Bechtle, O. Brein, S. Heinemeyer, G. Weiglein and K. E. Williams, *HiggsBounds:*
766 *confronting arbitrary Higgs sectors with exclusion bounds from LEP and the Tevatron*,
767 Comput. Phys. Commun. **181**, 138 (2010), doi:10.1016/j.cpc.2009.09.003, 0811.
768 4169.
- 769 [107] O. Stål and T. Stefaniak, *Constraining extended Higgs sectors with HiggsSignals*,
770 PoS **2013**, 314 (2013), doi:10.22323/1.180.0314, 1310.4039.
- 771 [108] P. Bechtle, S. Heinemeyer, O. Stål, T. Stefaniak and G. Weiglein, *Probing the Stan-*
772 *dard Model with Higgs signal rates from the Tevatron, the LHC and a future ILC*,
773 JHEP **1411**, 039 (2014), doi:10.1007/JHEP11(2014)039, 1403.1582.
- 774 [109] P. Bechtle, S. Heinemeyer, O. Stål, T. Stefaniak and G. Weiglein, *HiggsSignals:*
775 *Confronting arbitrary Higgs sectors with measurements at the Tevatron and the LHC*,
776 Eur. Phys. J. **C74**(2), 2711 (2014), doi:10.1140/epjc/s10052-013-2711-4, 1305.1933.
- 777 [110] G. Belanger, F. Boudjema, A. Pukhov and A. Semenov, *micrOMEGAs: Version 1.3*,
778 Comput. Phys. Commun. **174**, 577 (2006), doi:10.1016/j.cpc.2005.12.005, hep-ph/
779 0405253.
- 780 [111] G. Belanger, F. Boudjema, A. Pukhov and A. Semenov, *MicrOMEGAs 2.0: A*
781 *Program to calculate the relic density of dark matter in a generic model*, Comput.
782 Phys. Commun. **176**, 367 (2007), doi:10.1016/j.cpc.2006.11.008, hep-ph/0607059.

- 783 [112] G. Belanger, F. Boudjema, A. Pukhov and A. Semenov, *Dark matter direct detection*
784 *rate in a generic model with micrOMEGAs 2.2*, Comput. Phys. Commun. **180**, 747
785 (2009), doi:10.1016/j.cpc.2008.11.019, 0803.2360.
- 786 [113] G. Belanger, F. Boudjema, P. Brun, A. Pukhov, S. Rosier-Lees, P. Salati and A. Se-
787 menov, *Indirect search for dark matter with micrOMEGAs2.4*, Comput. Phys. Com-
788 mun. **182**, 842 (2011), doi:10.1016/j.cpc.2010.11.033, 1004.1092.
- 789 [114] G. Belanger, F. Boudjema, A. Pukhov and A. Semenov, *micrOMEGAs_3: A pro-*
790 *gram for calculating dark matter observables*, Comput. Phys. Commun. **185**, 960
791 (2014), doi:10.1016/j.cpc.2013.10.016, 1305.0237.
- 792 [115] G. Belanger, A. Mjallal and A. Pukhov, *Recasting direct detection limits within*
793 *micrOMEGAs and implication for non-standard Dark Matter scenarios* (2020),
794 2003.08621.
- 795 [116] M. Ackermann *et al.*, *Searching for Dark Matter Annihilation from Milky Way Dwarf*
796 *Spheroidal Galaxies with Six Years of Fermi Large Area Telescope Data*, Phys. Rev.
797 Lett. **115**(23), 231301 (2015), doi:10.1103/PhysRevLett.115.231301, 1503.02641.
- 798 [117] **The GAMBIT Dark Matter Workgroup**, *DarkBit: A GAMBIT module for*
799 *computing dark matter observables and likelihoods*, Eur. Phys. J. **C77**(12), 831
800 (2017), doi:10.1140/epjc/s10052-017-5155-4, 1705.07920.
- 801 [118] F. Mahmoudi, *SuperIso: A Program for calculating the isospin asymmetry of*
802 *$B \rightarrow K^* \gamma$ in the MSSM*, Comput. Phys. Commun. **178**, 745 (2008),
803 doi:10.1016/j.cpc.2007.12.006, 0710.2067.
- 804 [119] F. Mahmoudi, *SuperIso v2.3: A Program for calculating flavor physics ob-*
805 *servables in Supersymmetry*, Comput. Phys. Commun. **180**, 1579 (2009),
806 doi:10.1016/j.cpc.2009.02.017, 0808.3144.
- 807 [120] P. Athron, M. Bach, H. G. Fargnoli, C. Gnendiger, R. Greifenhagen, J.-h. Park,
808 S. Paßehr, D. Stöckinger, H. Stöckinger-Kim and A. Voigt, *GM2Calc: Precise*
809 *MSSM prediction for $(g - 2)$ of the muon*, Eur. Phys. J. C **76**(2), 62 (2016),
810 doi:10.1140/epjc/s10052-015-3870-2, 1510.08071.
- 811 [121] P. von Weitershausen, M. Schafer, H. Stockinger-Kim and D. Stockinger, *Photonic*
812 *SUSY Two-Loop Corrections to the Muon Magnetic Moment*, Phys. Rev. D **81**,
813 093004 (2010), doi:10.1103/PhysRevD.81.093004, 1003.5820.
- 814 [122] M. Bach, J.-h. Park, D. Stöckinger and H. Stöckinger-Kim, *Large muon $(g -$*
815 *2) with TeV-scale SUSY masses for $\tan\beta \rightarrow \infty$* , JHEP **10**, 026 (2015),
816 doi:10.1007/JHEP10(2015)026, 1504.05500.
- 817 [123] J. H. Kotecha and P. M. Djuric, *Gaussian particle filtering*, IEEE Transactions on
818 Signal Processing **51**(10), 2592 (2003), doi:10.1109/TSP.2003.816758.
- 819 [124] *LEP2 SUSY Working Group*, *ALEPH, DELPHI, L3 and OPAL experiments*.
- 820 [125] A. Heister *et al.*, *Absolute lower limits on the masses of selectrons and sneutrinos*
821 *in the MSSM*, Phys. Lett. B **544**, 73 (2002), doi:10.1016/S0370-2693(02)02471-1,
822 hep-ex/0207056.

- 823 [126] M. Carena, A. de Gouvea, A. Freitas and M. Schmitt, *Invisible Z boson decays at*
824 *e^+e^- colliders*, Phys. Rev. **D68**, 113007 (2003), doi:10.1103/PhysRevD.68.113007,
825 0308053.
- 826 [127] T. Han, Z. Liu and A. Natarajan, *Dark matter and Higgs bosons in the MSSM*,
827 JHEP **11**, 008 (2013), doi:10.1007/JHEP11(2013)008, 1303.3040.
- 828 [128] G. Belanger, F. Boudjema, A. Cottrant, R. M. Godbole and A. Semenov, *The MSSM*
829 *invisible Higgs in the light of dark matter and $g-2$* , Phys. Lett. B **519**, 93 (2001),
830 doi:10.1016/S0370-2693(01)00976-5, hep-ph/0106275.
- 831 [129] T. Nihei, L. Roszkowski and R. Ruiz de Austri, *Exact cross-sections for the neutralino*
832 *slepton coannihilation*, JHEP **07**, 024 (2002), doi:10.1088/1126-6708/2002/07/024,
833 hep-ph/0206266.
- 834 [130] M. Aaboud *et al.*, *Search for chargino-neutralino production using recursive jigsaw*
835 *reconstruction in final states with two or three charged leptons in proton-proton colli-*
836 *sions at $\sqrt{s} = 13$ TeV with the ATLAS detector*, Phys. Rev. D **98**(9), 092012 (2018),
837 doi:10.1103/PhysRevD.98.092012, 1806.02293.
- 838 [131] A. M. Sirunyan *et al.*, *Combined search for electroweak production of charginos and*
839 *neutralinos in proton-proton collisions at $\sqrt{s} = 13$ TeV*, JHEP **03**, 160 (2018),
840 doi:10.1007/JHEP03(2018)160, 1801.03957.
- 841 [132] A. M. Sirunyan *et al.*, *Search for supersymmetry in final states with two oppositely*
842 *charged same-flavor leptons and missing transverse momentum in proton-proton colli-*
843 *sions at $\sqrt{s} = 13$ TeV* (2020), 2012.08600.
- 844 [133] A. M. Sirunyan *et al.*, *Search for supersymmetry with a compressed mass*
845 *spectrum in the vector boson fusion topology with 1-lepton and 0-lepton final*
846 *states in proton-proton collisions at $\sqrt{s} = 13$ TeV*, JHEP **08**, 150 (2019),
847 doi:10.1007/JHEP08(2019)150, 1905.13059.
- 848 [134] *Search for electroweak production of charginos and neutralinos in proton-proton colli-*
849 *sions at $\sqrt{s}=13$ TeV*, Tech. Rep. CMS-PAS-SUS-19-012, CERN, Geneva (2021).
- 850 [135] M. Aaboud *et al.*, *Search for the direct production of charginos and neutralinos in*
851 *final states with tau leptons in $\sqrt{s} = 13$ TeV pp collisions with the ATLAS detector*,
852 Eur. Phys. J. C **78**(2), 154 (2018), doi:10.1140/epjc/s10052-018-5583-9, 1708.07875.
- 853 [136] A. M. Sirunyan *et al.*, *Search for direct pair production of supersymmetric partners*
854 *to the τ lepton in proton-proton collisions at $\sqrt{s} = 13$ TeV*, Eur. Phys. J. C **80**(3),
855 189 (2020), doi:10.1140/epjc/s10052-020-7739-7, 1907.13179.
- 856 [137] A. M. Sirunyan *et al.*, *Search for Supersymmetry with a Compressed Mass Spectrum*
857 *in Events with a Soft τ Lepton, a Highly Energetic Jet, and Large Missing Transverse*
858 *Momentum in Proton-Proton Collisions at $\sqrt{s} = 13$ TeV*, Phys. Rev. Lett. **124**(4),
859 041803 (2020), doi:10.1103/PhysRevLett.124.041803, 1910.01185.
- 860 [138] G. Aad *et al.*, *Search for direct stau production in events with two hadronic τ -leptons*
861 *in $\sqrt{s} = 13$ TeV pp collisions with the ATLAS detector*, Phys. Rev. D **101**(3), 032009
862 (2020), doi:10.1103/PhysRevD.101.032009, 1911.06660.

- 863 [139] G. Aad *et al.*, *Searches for electroweak production of supersymmetric particles with*
864 *compressed mass spectra in $\sqrt{s} = 13$ TeV pp collisions with the ATLAS detector*,
865 *Phys. Rev. D* **101**(5), 052005 (2020), doi:10.1103/PhysRevD.101.052005, 1911.
866 12606.
- 867 [140] G. Aad *et al.*, *Search for electroweak production of charginos and sleptons decaying*
868 *into final states with two leptons and missing transverse momentum in $\sqrt{s} = 13$*
869 *TeV pp collisions using the ATLAS detector*, *Eur. Phys. J. C* **80**(2), 123 (2020),
870 doi:10.1140/epjc/s10052-019-7594-6, 1908.08215.
- 871 [141] J. Kumar and D. Marfatia, *Matrix element analyses of dark matter scattering and*
872 *annihilation*, *Phys. Rev.* **D88**(1), 014035 (2013), doi:10.1103/PhysRevD.88.014035,
873 1305.1611.
- 874 [142] *Toward a next-generation dark matter search with the PICO-40L bubble chamber*,
875 [https://indico.cern.ch/event/606690/contributions/2623446/attachments/](https://indico.cern.ch/event/606690/contributions/2623446/attachments/1497228/2330240/Fallows_2017_07_24__TAUP__PICO-40L_v1.2.pdf)
876 [1497228/2330240/Fallows_2017_07_24__TAUP__PICO-40L_v1.2.pdf](https://indico.cern.ch/event/606690/contributions/2623446/attachments/1497228/2330240/Fallows_2017_07_24__TAUP__PICO-40L_v1.2.pdf), Accessed:
877 2021-03-24.
- 878 [143] D. S. Akerib *et al.*, *LUX-ZEPLIN (LZ) Conceptual Design Report* (2015), 1509.
879 02910.